Evidence for influenza B virus hemagglutinin adaptation to the human host: high cleavability, acid-stability and preference for cool temperature

Manon Laporte[1], Annelies Stevaert[1], Valerie Raeymaekers[1], Talitha Boogaerts[1], Inga Nehlmeier[2], Winston Chiu[1], Mohammed Benkheil[1], Bart Vanaudenaerde[3], Stefan Pöhlmann[2,4] and Lieve Naesens[1*]

[1] KU Leuven–University of Leuven, Department of Microbiology and Immunology, Rega Institute for Medical Research, Laboratory of Virology and Chemotherapy, Leuven, Belgium

[2]Infection Biology Unit, German Primate Center–Leibniz Institute for Primate Research, Göttingen, Germany

[3]KU Leuven–University of Leuven, Department of Chronic Diseases, Metabolism and Ageing, Laboratory of Pneumology, University Hospital Leuven, Leuven, Belgium

[4]Faculty of Biology and Psychology, University Göttingen, Göttingen, Germany

* Corresponding author

E-mail: lieve.naesens@kuleuven.be

Abstract

Influenza A virus (IAV) and influenza B virus (IBV) cause yearly epidemics associated with significant morbidity and mortality. Whereas IBV is confined to humans, IAV circulates in animal reservoirs from where it can enter the human population. When this occurs, adaptation of the viral hemagglutinin (HA) is required to achieve sustained human-to-human transmission. IBV has been circulating in humans for a long period of time. Whether this entailed adaptation of IBV HA to the human host is unknown. To address this question, we compared the two seasonal IAV (A/H1N1 and A/H3N2) and two IBV viruses (B/Victoria and B/Yamagata lineage) with regard to host-dependent activity of HA as the mediator of membrane fusion during viral entry. First, we investigated host cell protease-dependent activation of HA, required to render HA membrane fusion-competent. Our analysis covered all members of the type II transmembrane serine protease (TTSP) and kallikrein families, many of which proved to be expressed in human respiratory epithelium. We found that, compared to IAV, the IBV HA0 precursor is cleaved by a broader panel of TTSPs and is activated with much higher efficiency. In agreement with this finding, knockdown of a single HA-processing enzyme, TMPRSS2, was sufficient to abrogate spread of IAV but not IBV in human airway epithelial cells. Second, we showed that the acidic pH required to trigger membrane fusion by HA is similar for IBV and human-adapted IAVs (one noticeable exception being the HA of 1918 IAV), indicating that IBV HA is well-adapted to resist the mildly acidic pH in the upper part of the human respiratory tract. Finally, IBV HA exhibited higher protein expression at 33°C than at 37°C, and 33°C was strictly required to achieve membrane fusion driven by HA of the B/Victoria lineage. Preference for a cooler temperature fits with adaptation of IBV to the proximal airways. In sum, we revealed some distinct properties of the IBV HA protein, which are compatible with extensive adaptation to the human airways during prolonged circulation of IBV in the human population.

Author summary

The yearly influenza epidemics are caused by influenza A (IAV) and influenza B (IBV) viruses. IBV predominates in some seasons and causes substantial disease, however it is far less studied than IAV. While IAV originates from animal reservoirs, IBV circulates in humans only. To allow virus spread, the hemagglutinin (HA) protein that is present at the surface of influenza virus particles should be active and sufficiently stable in the conditions of human airways. We here resolve how these mechanisms differ between IBV and IAV. Whereas human IAVs heavily rely on one particular protease for HA activation, this is not the case for IBV. Superior activation of IBV by a broader range of airway proteases should enhance shedding of infectious virus particles. The IBV HA protein exhibits acid-stability and a preference for 33°C. These two properties indicate optimal adaptation to the upper part of the human respiratory tract, where the pH is mildly acidic and a cooler temperature exists. These adaptive features can be rationalized by the long existence of IBV in the human species, and may have broader relevance for understanding the biology and evolution of respiratory viruses.

Introduction

The global burden of seasonal influenza is estimated at 3 to 5 million severe cases (1) and 290,000-650,000 fatalities per year (2). In addition, influenza A virus (IAV) causes intermittent pandemics with an even more severe impact on public health. Influenza B virus (IBV) does not cause pandemics but is responsible for a significant proportion of seasonal influenza (3). IBV may account for 22-44% of influenza deaths in children (3) and also elderly persons are at high risk (4). Between 1997 and 2009, IBV was the predominant cause of influenza-associated death in 4 out of 12 seasons (5). The divergence between IAV and IBV was estimated to have occurred 4,000 years ago (6) and about 40 years ago, IBV diverged into two lineages, B/Victoria and B/Yamagata, which are now cocirculating globally (7). Gene reassortment between the two lineages is common yet not seen for the HA, PB1 and PB2 gene segments (7). Whereas IAV is widespread in birds and mammals (8), IBV is restricted to humans with no sustained animal reservoir (9) and only rare cross-over events (10).

The trimeric influenza virus hemagglutinin (HA) facilitates viral entry into target cells (11, 12). For this, HA binds to sialylated glycoproteins or glycolipids on the cell surface, which results in virus uptake by endocytosis. Next, HA mediates fusion of the viral envelope and endosomal membrane, allowing release of the viral genome into the cytoplasm. Membrane fusion occurs when virus-containing endosomes mature from early (pH ~6) to late (pH ~5) endosomes, providing the low pH trigger for drastic refolding of HA and expulsion of its fusion peptide (13). In order to become membrane fusion-competent, the HA0 precursor protein relies on host cell proteases for posttranslational cleavage into two polypeptides, HA1 and HA2, a process termed priming or, for historical reasons, activation (14). In human IAV and IBV strains, HA0 has a monobasic (single arginine) cleavage site that is recognized by trypsin-like serine proteases. Insight into which proteases are involved in HA activation may help to understand potential differences between IAV and IBV, and guide novel therapeutic strategies targeting HA-activating airway proteases (15, 16). Studies of the last decade (reviewed by Böttcher-

Friebertshäuser *et al*. (17)) have linked a series of proteases to IAV HA activation, but for IBV hardly any information is available. The type II transmembrane serine protease (TTSP) TMPRSS2 (transmembrane protease serine 2) cleaves IAV HA0 in cell culture, is expressed in human airways and is essential for IAV replication in mice, at least for contemporary A/H1N1, avian A/H7N9 and an H10-reassorted IAV (18-21). In humans, a gene polymorphism leading to higher *TMPRSS2* expression has been associated with increased risk for severe influenza (22). A few other TTSPs and some kallikreins can also activate IAV in cell culture, but which of these enzymes support spread of IAV in human airways is still unknown [reviewed in: (15, 23)]. Regarding IBV, TMPRSS2 was shown to cleave IBV HA0 in cell culture (16), but to be dispensable for IBV spread and pathogenesis in mice (24). Which airway protease(s) activate IBV HA in the infected host is unknown.

A second determinant of HA activity is its acid-stability. Successful virus replication and transmission require a balance between the low pH that triggers HA refolding and membrane fusion during virus entry, and acid-stability of progeny virus in the respiratory tract and environment (25, 26). Extracellular virions are sensitive to inactivation in mildly acidic parts of the upper respiratory tract (URT) like the nasal cavity (25, 27, 28). The acid-stability of HA appears to increase when a zoonotic IAV enters the human population and evolves into a human-to-human transmissible strain (29, 30). Studies in ferrets showed that increased HA acid-stability contributes to airborne transmissibility (29, 31, 32). Whether IBV HA is optimally adapted to an acidic environment has not been addressed before.

A temperature gradient exists in the human airways, from ~30-32°C in the nasal mucosa (33), to ~32°C in the upper trachea and ~36°C in the bronchi (34). Avian IAVs, adapted to the temperature of the avian enteric tract (40°C) show restricted growth at cooler temperatures. Temperature-dependent activity of the viral polymerase, related to the 627 signature residue in the PB2 subunit, is an important determinant of temperature sensitivity (35, 36). However, also the viral surface glycoproteins, HA and neuraminidase, contribute to the restricted growth

of avian IAVs at 32°C (37). Whether HA proteins from human IAV or IBV have a preference for the cooler temperatures of the human URT (30-32°C) is not clear.

In the present study, we compared the HA proteins of four seasonal human IAV and IBV viruses to understand how their membrane fusion activity is dependent on human airway-related host factors. Activation by human proteases was analyzed by covering all members of the TTSP (38) and kallikrein (KLK) families (39) families. We demonstrate that IBV HA displays more efficient activation by airway proteases than IAV HA. TMPRSS2 was required for spread of IAV but not IBV in human respiratory epithelial cells. The HA proteins of IBV and human IAV showed similar low pH-dependence to trigger membrane fusion. Besides, we found that IBV HA prefers a temperature of 33°C and that one of the two IBV lineages requires this cooler temperature to induce membrane fusion. We propose that the distinct properties of the IBV HA protein might reflect adaptation of this pathogen to the human respiratory tract.

Results

Human lung tissue and airway epithelial cell lines are rich in TTSP and KLK enzymes

Activation by one or more airway proteases is crucial to render the IAV and IBV HA proteins membrane fusion-competent. We first assessed which TTSPs and KLKs are expressed in human airways. Hence, we quantified their mRNA levels in tissue samples of healthy human lungs (Figs 1A and 1B) and three continuous cell lines (Calu-3, 16HBE and A549) derived from human airways (Figs 1C and 1D). The four TTSP subfamilies are indicated at the top of Figs 1A and 1C. Lung tissue samples from eight different donors contained high transcript levels for *TMPRSS2* and *ST14/matriptase*, followed by *TMPRSS3, TMPRSS4, TMPRSS5, TMPRSS6, TMPRSS11D/HAT, TMPRSS11E/DESC1, TMPRSS11A, TMPRSS13/MSPL*, *Hepsin (HPN) and Corin* (Fig 1A: left). These results agreed with microarray data obtained from 108 healthy human lungs, retrieved from the GEO database, in which high mRNA levels were observed for *Hepsin*, *TMPRSS2, TMPRSS3, TMPRSS6, TMPRSS13/MSPL, ST14/matriptase* and *Corin* (Fig 1A: right). Human lung tissue was also found to contain high mRNA levels for several KLKs, but expression was in general more variable compared to the TTSP transcripts (compare right panels of Figs 1A and 1B). Calu-3 and 16HBE cells (Figs 1C and 1D) showed abundant expression of *ST14/matriptase.* Besides, Calu-3 cells expressed high levels of *TMPRSS2, TMPRSS3* and *TMPRSS4* mRNA*.* Both cell lines also expressed a range of *KLK* transcripts, particularly *KLK5, KLK6, KLK7, KLK10 and KLK11*. Protease expression in A549 and HEK293T cells was generally lower compared to Calu-3 and 16HBE cells (Fig 1E). Finally, furin (which recognizes multibasic HA0 cleavage sites of highly pathogenic avian IAVs (40)) was abundantly expressed in the four cell lines and human lung tissue (data not shown), as expected from previous work (41).

IBV HA0 is efficiently cleaved by a broad range of TTSPs

The variety of TTSP and KLK enzymes expressed in human lungs and airway epithelial cells raised the question which of these proteases can activate the HA proteins of IAV or IBV.

Expression plasmids were generated for all 18 known TTSP family members and 16 KLKs, bearing a C-terminal flag tag (for details see S1 Table). When we analyzed their expression in transfected cells, most proteases showed a protein level similar to that of TMPRSS2 regarded as the reference (S1 Fig C). For TMPRSS11B, -12, -7 and KLK13, expression was three-fold lower. For TMPRSS11D/HAT and TMPRSS11E/DESC1 expression was very weak, meaning that the results obtained in the HA cleavage assay are an underestimate for these two proteases. In this assay, the proteases were co-expressed with the HAs from four seasonal IAV (A/H1 and A/H3) and IBV (B/Yam and B/Vic) viruses (Fig 2A). HA0 cleavage was assessed by western blot for the HA1 or HA2 cleavage product, depending on which epitope was recognized by the anti-HA antibody. The % cleaved HA was calculated relative to the trypsin control, consisting of cells transfected with HA plus empty plasmid, and briefly exposed to exogenous trypsin.

TMPRSS2 was the only protease that efficiently cleaved all four IAV/IBV HA0 proteins tested. It was the only protease with high activity on A/H3 HA (Fig 2B and 2C). In the case of A/H1 HA, TMPRSS4 proved equally effective as TMPRSS2, while cleavage by TMPRSS11F and TMPRSS6 was less efficient. On the other hand, both IBV HA0 proteins were effectively cleaved by a broader range of TTSPs (Fig 2B and 2C). Namely, TMPRSS4, TMPRSS11F and TMPRSS13/MSPL generated equal or higher levels of cleaved IBV HA as TMPRSS2, and also TMPRSS11A proved effective. We also detected HA0 cleavage by TMPRSS11D/HAT, yet low expression of this protease (see above) precluded conclusions on cleavage efficiency. In addition, the B/Yam HA0 protein was efficiently processed by Hepsin, TMPRSS5 and TMPRSS6. Hepsin generated weak bands for both HA0 and HA1/HA2 (Fig 2B), indicating HA degradation as observed before (42). Finally, none of the kallikreins was found to be a broad HA activator. KLK14 cleaved both IBV proteins, whereas KLK5 and KLK6 cleaved B/Yam HA0 with low efficacy. In summary, we demonstrated that, compared to its IAV counterpart, IBV HA0 can use a broader panel of TTSPs for its proteolytic cleavage.

All HA0-cleaving TTSPs generate membrane fusion-competent IBV HA

We next examined whether HA0 cleavage translates into HA activation. For this, we first employed a polykaryon assay in which HeLa cells that co-express HA and protease are exposed to acidic pH to trigger HA-mediated cell-cell fusion (Fig 3A). We ensured that the four HAs were compared with similar stringency, i.e. at a pH 0.1 unit below their fusion pH (see below). Abundant polykaryons were produced when IAV or IBV HA was co-expressed with TMPRSS11F, TMPRSS2, TMPRSS4, and TMPRSS13/MSPL, and to a lesser extent with TMPRSS11D/HAT, TMPRSS11A, Hepsin, TMPRSS5 and TMPRSS6 (Fig 3B and C). All these TTSPs thus generate a fusion-competent HA1-HA2 protein, meaning that they cleave HA0 at the correct position. The quantitative differences in HA0 processing among the TTSPs, seen by western blot analysis, were not fully reflected in the polykaryon assay, most likely because a few activated HAs are sufficient to induce cell-cell fusion (43, 44). No polykaryons were formed in cells expressing KLK5, KLK6 or KLK14 (Fig 3B and C). For KLK5 and KLK6, the levels of cleaved HA (Fig 2) were probably too low to induce membrane fusion. KLK14 likely cleaves the B/Yam and B/Vic HA0 proteins at an incorrect position, since the HA2 product generated by KLK14 migrated slightly slower (Fig 2B) than that produced by trypsin or an activating TTSP.

A broad range of TTSPs efficiently activates IBV HA for membrane fusion during virus entry

We next examined whether the HA0-cleaving TTSPs generate a functional HA that enables virus entry. For this, we employed a retroviral pseudotyping system with luminescence readout (Fig 4A). Each HA was combined with its cognate neuraminidase (NA) to assure efficient particle release (45, 46). Particles were produced in the presence or absence of TTSPs, treated with PBS or trypsin and then examined for their ability to transduce target cells (Fig 4A). In Fig 4B and 4C, the colored bars show the transduction efficiency of TTSP-activated particles, whereas the white bars show total particle infectivity upon additional treatment with trypsin.

For the two seasonal IAVs, pseudoparticles produced in the presence of TMPRSS2 and TMPRSS11D/HAT (now generated from the pCAGGS plasmid to bypass low expression; see above) transduced cells with the same efficiency as trypsin-treated control particles (indicated with the dashed line in Figs 4B and 4C). A/H1 HA, but not A/H3 HA, was also fully activated by TMPRSS4. Accordingly, transduction efficiency of these particles was only slightly increased when they were treated with trypsin. In sharp contrast, IBV HA-bearing pseudotypes produced in the presence of Hepsin, TMPRSS2, TMPRSS4, TMPRSS13/MSPL, TMPRSS11D/HAT and TMPRSS11E/DESC1 (for B/Yam), transduced cells with markedly higher efficiency than control particles treated with trypsin (Fig 4B). For instance, B/Yam particles activated by TMPRSS2 or TMPRSS11D/HAT generated approximately 2000-fold higher signals than the trypsin control. The superior activation of the IBV particles was also evident from the observation that, for most TTSPs, subsequent trypsin treatment gave a lower signal increase for the IBV compared to the IAV particles (see white bars in Fig 4B).

To investigate the possibility that the efficiency of HA activation might be linked to IAV virulence or pandemic potential, we included pseudotypes derived from 1918 A/H1N1 IAV and avian A/H7N9 IAV, which both possess a monobasic HA0 cleavage site. The former virus caused the devastating 1918 pandemic, and its HA protein was identified as a virulence determinant (47, 48) although the underlying mechanism is not understood (49, 50). A high case-fatality rate in humans is also seen with avian A/H7N9 IAV, which is feared for its pandemic potential (51). The three A/H1N1 pseudotypes tested, i.e. derived from 1918 IAV, 2009 pandemic virus and the laboratory strain A/PR/8/34 (PR8) as well as the A/H7N9 subtype shared TMPRSS2 and TMPRSS4 as the most effective HA-activators, showing comparable efficiency as the trypsin control (Fig 4C). Hence, whereas TTSP-mediated HA activation was clearly more efficient for IBV compared to IAV pseudotypes, such a difference was not seen for highly virulent *versus* seasonal IAVs. On the other hand, pseudoparticles carrying 1918 HA and NA showed 10- and 100-fold higher transduction efficiency than the PR8 and Virg09-pseudotypes, respectively (S2 Fig). Since the three A/H1N1 pseudotypes showed comparable incorporation

of HA and MLV gag and a similar level of HA0 cleavage (S2 Fig), the difference might be related to the HA fusion pH (see below) (26). An alternative explanation may be that the 1918 IAV neuraminidase, present in these pseudoparticles, may have enhanced their entry process (52).

To summarize, the results from the HA functional polykaryon and pseudoparticle assays established ten TTSPs as moderate to strong activators of HA, with IBV HA being particularly well activated by a broader range of TTSPs than that used by IAV HA, including three HA0-activators (TMPRSS5, TMPRSS6 and TMPRSS11F) not recognized before.

IBV but not IAV can employ several proteases for spread in human airway-derived Calu-3 cells

As shown in Fig 1E, the TTSP and KLK expression profile in Calu-3 cells proved similar to that seen in healthy human lungs. Thus, Calu-3 cells are a good model to study the role of TTSP and KLK enzymes in virus activation in the human respiratory tract. For the four IAV/IBV strains studied, i.e. Virg09 (A/H1N1), HK68 (A/H3N2), Ned05 (B/Yam) and Mal04 (B/Vic), multicycle (i.e. zanamivir-sensitive, S5 Table) replication in Calu-3 cells was indistinguishable irrespective of exogenous trypsin (*P*-value > 0.1, S3 Fig), indicating that these cells express one or more HA0-activating proteases. The four viruses were similarly inhibited by three serine protease inhibitors (see antiviral EC_{50} values in S5 Table; a brief description of the assay is provided below this Table) but were not blocked by a furin inhibitor, consistent with furin's inability to process monobasic HA0 cleavage sites (40). We also observed no effect with inhibitors of lysosomal cathepsins, which can activate diverse emerging viruses (53). Thus, HA activation in Calu-3 cells depends on the activity of one or more serine proteases.

After optimizing the procedure for robust siRNA-mediated gene knockdown in Calu-3 cells (S4 Fig), we performed broad knockdown for the 18 TTSPs and 16 KLKs. To assess the impact of protease knockdown on IAV or IBV replication, virus was added 48 h after siRNA transfection, and virus infection was monitored at day 3 p.i. by high-content imaging of NP immunostaining (Fig 5A). We first ascertained that neither of the siRNAs produced unwanted cytotoxic effects,

the only exception being TMPRSS6 knockdown which reduced cell viability by 40% (Fig 5B). TMPRSS2 was the only protease for which knockdown caused significant (*P*-value = 0.0001) reduction in replication of A/H1N1 and A/H3N2 virus (Fig 5B and 5C). In sharp contrast, IBV infection was only marginally (Fig 5B, B/Yam: *P*-value = 0.047) or not (Fig 5B, B/Vic: *P*-value = 0.48) reduced by TMPRSS2 knockdown. Finally, IBV was not markedly affected by either of the individual siRNAs or combined knockdown of TMPRSS2 and the most efficacious IBV HA activators identified above (Fig 5D). Hence, IBV appears to rely on various proteases to replicate in human respiratory epithelial cells, concurring with the above findings that, besides TMPRSS2, several proteases effectively activate the IBV HA protein.

MDCK cells contain high levels of HA-cleaving TMPRSS4 but this protease is dispensable for trypsin-independent spread of IBV

To assess which TTSPs might stand out as IBV HA-activators, we used Madin-Darby canine kidney (MDCK) epithelial cells which, alike Calu-3 cells, support replication of IBV in the absence of trypsin (54). This observation was also made for 1918 IAV (52, 55) which, in this regard, is unique among human IAV strains. Indeed, our seasonal IBV but not IAV viruses did not require exogenous trypsin to replicate in MDCK cells (Fig 6A). HA0 cleavage during IBV replication was inhibited by the broad serine protease inhibitor camostat (Fig 6B), hence executed by one or more members of this protease family. To identify these factors in MDCK cells, we measured mRNA levels for the IBV HA0-cleaving TTSPs and KLKs identified in the previous part, using dog-specific primers (S3 Table). Besides high expression of *ST14/matriptase* as observed before (56, 57), we detected a very high level of *TMPRSS4* mRNA (Fig 6C). This opposes another study (52) reporting no *TMPRSS4* transcription in MDCK cells, potentially related to the use of different MDCK cell lines (58). We next created an expression plasmid for MDCK cell-derived TMPRSS4 to investigate its HA0-cleaving capacity. Three plasmid concentrations were applied to vary the level of protease. Canine TMPRSS4 proved a strong activator for the B/Yam, B/Vic and 1918 A/H1 HAs (Fig 6D). It had lower efficiency against A/H1 (Virg09) HA, and, especially, A/H3 HA. The polykaryon assay in

HeLa cells confirmed that canine TMPRSS4 produces fusion-competent HA (pictures in Fig 6D).

Next, the role of canine TMPRSS4 was assessed by siRNA-mediated knockdown. We included siRNA for ST14/matriptase, also abundantly expressed in MDCK cells. For IAV, published data on the role of matriptase in activation of HA are not consistent (57, 59, 60). Although our HA cleavage and functional analysis from above did not support a direct role for matriptase, an indirect role (e.g. as an activator of TMPRSS4) could not be excluded. With this is mind, we performed knockdown for canine TMPRSS4 and matriptase individually or in combination (Fig 6E and 6F). Knockdown efficiency was >85% based on RT-qPCR for mRNA. Virus replication and HA0 cleavage in IBV-infected MDCK cells proved unaffected by knockdown of TMPRSS4, matriptase, nor a combination of the two (Fig 6F). Thus, both in Calu-3 and MDCK cells, no single protease was identified as a dominant player in IBV replication.

IBV HA exhibits a similar fusion pH as human-adapted IAV HAs

Cleavage of HA0 into HA1-HA2 activates the protein for membrane fusion, but also generates a metastable protein that is sensitive to inactivation at acidic pH. The nasal cavity of humans is mildly acidic (average 6.3 in healthy adults and 5.9 in children) (28, 61). For IAV, acquirement of a more acid-stable HA is considered a prerequisite to achieve human-to-human transmissibility (25, 29, 45, 62). Given that IBV is restricted to humans, we asked whether IBV possesses an acid-stable HA. Indeed, the polykaryon assay showed that the two IBV HA (i.e. B/Yam and B/Vic) proteins studied have a fusion pH value in the same range (5.4-5.6) as their human IAV counterparts (Fig 7B-D), while avian A/H5 and A/H7 HAs had higher values (5.7 and 5.8, respectively; Fig 7E), in line with previous reports (32, 45, 63, 64). Intriguingly, 1918 A/H1 HA (Fig 7D) had the highest fusion pH among the tested human IAV HAs, its value (5.7) being as high as avian A/H5 HA (Fig 7E). This might explain the superior transduction efficiency of 1918 IAV pseudoparticles in HEK293T cells (see above), since an increased fusion pH enables earlier endosomal escape and thus more efficient infection (26). Although

IBV HA exhibited a similar fusion pH as human-adapted IAVs, a difference was noticed in the shape of the pH curves. For the IAV HAs, the curves showed a discrete pH value at which the number of polykaryons was maximal, and a steep decline at more acidic pH due to HA inactivation (65). In contrast, both IBV HAs produced high numbers of polykaryons over the entire low pH range tested (4.9-5.3 in case of B/Vic HA and 4.9-5.5 in case of B/Yam HA). Hence, cleaved IBV HA is triggered for fusion at a similar acidic pH as IAV HA, however the IBV protein may be more resistant to acidic conditions.

A temperature of 33°C is preferred by IBV HA and required for fusion by the B/Victoria lineage

The human URT has a temperature (~30-32°C) below body temperature (33, 34) and well below that of the avian intestinal tract (~40°C) (35, 66). Since a temperature of 33°C is preferred for propagating IBV in cell culture, we investigated whether HA has a role in this temperature preference. The expression of IBV HA in HeLa cells proved to be temperature-dependent, being highest at 33°C and gradually decreasing at higher temperatures (Fig 8A). The 33°C preference was seen for both IBV lineages but was particularly significant for B/Vic HA (*P*-value = 0.0006 for comparison of protein levels at 33°C and 37°C). For human IAV and avian A/H5 HAs, expression was similar within the range of 33-39°C, although for A/H1 HAs, it tended to be highest at 39°C. Avian A/H7 HA manifested a clear preference for 39°C (Fig 8A).

For B/Vic HA, the low protein levels at 37°C resulted in inability to induce membrane fusion in the polykaryon assay at any pH tested (Fig 8D), while abundant polykaryons were formed at 33°C (Fig 8B and 8C). Varying the temperature during protein expression or membrane fusion (see arrow schemes in Fig 8B) revealed that this 33°C requirement was due to inefficient HA expression at 37°C. Whether cell-cell fusion took place at 33°C or 37°C made no difference. Due to this low expression at 37°C, the levels of activated HA, generated by trypsin, were undetectable (Fig 8D). Likewise, B/Vic pseudoparticles produced at 37°C had much lower infectivity compared to those generated at 33°C (*P*-value < 0.0001, Fig 8E). At this cooler

temperature, higher HA protein levels were visible, particularly in released pseudoparticles (Fig 8E), suggesting that this reduced temperature may be required for efficient posttranslational transport and membrane incorporation of B/Vic HA.

The strict 33°C requirement was not seen with B/Yam HA, since this protein generated polykaryons at all temperatures, including at 39°C (Fig 8B). The HA of the B/Vic lineage carries a globular head glycan at residue N248, that is lacking in the B/Yam lineage (7, 67, 68). To assess the role of this N-glycan in the different temperature requirements of the B/Vic and B/Yam HAs, we replaced N248 in B/Vic HA by D248, the corresponding residue in B/Yam HA. This substitution caused a shift from 5.4 to 5.5 in the pH threshold to induce polykaryons (Fig 8C). Furthermore, polykaryons induced by the N248D-mutant were larger and more numerous compared to wild-type B/Vic HA (Fig 8B and 8C). However, the mutation did not change the 33°C preference for protein expression and dependence on this temperature to induce membrane fusion (Fig 8B-D), indicating that the N248 glycan is not responsible for the temperature-sensitive phenotype of B/Vic HA.

In combination, these results indicate a possible correlation between HA expression and host temperature, with IBV HA preferring 33°C, the temperature of the human URT, and avian A/H7 HA preferring the body temperature of birds. The 33°C preference was stricter for B/Vic HA than for B/Yam HA, a difference unrelated to the lineage-specific N248 glycan.

Discussion

Compared to the large body of literature on the HA proteins from human and zoonotic IAVs and how some of their properties reflect viral host-adaptation (recently reviewed in (8, 25)), the HA of IBV is far less characterized (9). In this study, we compared the HA proteins of human IAV and IBV in terms of proteolytic activation, pH stability and temperature preference, as markers for host adaptation. Our results provide evidence for more pronounced adaptation of IBV HA to the human airways, in keeping with the long and exclusive circulation of IBV in humans.

In order to be membrane fusion-competent, HA requires cleavage by a host cell protease. Several TTSPs and KLKs were linked to IAV HA activation in separate reports (reviewed in (17)), yet a comprehensive analysis was, thus far, missing for IAV and especially for IBV. To close this gap, we compared all 18 human TTSP and 16 KLK enzymes for their capacity to cleave and activate the IAV and IBV HA proteins. Our results confirm the leading role of TMPRSS2 in activation of monobasic IAV HAs, consistent with data obtained in cell culture, knockout mice or humans (18, 19, 22). The report that TMPRSS2 proved dispensable for IBV spread and pathogenesis in mice (24) suggested that either TMPRSS2 is not involved at all in IBV HA activation or that several proteases may activate IBV HA. Our findings indicate that the latter assumption may be true, since the cleavability of IBV HA proved to be superior to that of IAV. We demonstrated that the HA proteins of the two IBV lineages are cleaved and activated by a broad range (in total ten) TTSP enzymes, the strongest activators being TMPRSS2, TMPRSS4, TMPRSS11F, TMPRSS13/MSPL, Hepsin and TMPRSS11D/HAT, followed by four other proteases (TMPRSS5, TMPRSS6, TMPRSS11A, TMPRSS11E/DESC1). All these TTSPs proved to be expressed in human lung tissue and to generate a functional, i.e. membrane fusion-competent, HA protein. In contrast, efficient activation of A/H1N1 and A/H3N2 HA was largely limited to TMPRSS2 and TMPRSS11D/HAT, and TMPRSS4 in the case of A/H1N1. Unlike others, we saw no evidence for a role of TMPRSS15/enterokinase

(Hayashi 2018) or KLK5, KLK12 (69, 70) or any other kallikrein. It is possible that the KLK levels attained in our cell systems were below those applied during incubation with recombinant KLKs (69). Finally, our data do not support the proposed involvement of ST14/matriptase in cleavage of A/H1 HA (59, 60), but agree with another report (57).

The efficient and broad activation of IBV HA explains why knockdown of any of the 18 TTSPs had no impact on IBV replication in Calu-3 cells, a human airway-derived cell line with a similar TTSP expression profile as human lung tissue. Similarly, dual knockdown of TMPRSS2 plus another HA-activating TTSP did not alter IBV replication. In contrast, replication of A/H1N1 and A/H3N2 viruses was strongly dependent on TMPRSS2. This is noteworthy considering that TMPRSS4 efficiently activated A/H1 HA in transfected cells and proved abundantly expressed in Calu-3 cells. Why does TMPRSS2 play a central role in activation of IAV HA? TMPRSS2 but not other HA-activating TTSPs may be expressed at high levels in all compartments of the constitutive secretory pathway (71) and may thus be present at higher levels at the site of HA activation. Similarly, only TMPRSS2 might show extensively colocalization with HA (72). Finally, TMPRSS2 might not only be required for activation of HA but also of M2 (73). Why is IBV HA more efficiently activated than IAV HA? It is conceivable that IBV HA may exhibit higher TTSP accessibility, perhaps governed by the dynamics of HA glycoprotein folding, maturation, or transport towards the cell membrane. This might be influenced by *N*-glycans in the HA head or stem (at sites very distant from the cleavage loop) having an effect on HA folding rate (74). An *N*-glycan (N8) located at the bottom of the A/H3 HA stem was shown to retard HA folding (74) and be lost when an A/H3N2 virus was passaged in TMPRSS2-knockout mice (75). Another factor is the HA0 cleavage site itself, for which two differences between IBV and IAV may be relevant: (i) at position P3 (P1 being the scissile arginine), IBV HA0 contains an extra basic lysine residue while A/H1 and A/H3 HAs carry a glutamine; and (ii) the P2’ residue is phenylalanine in IBV but leucine, a less hydrophobic residue, in human IAV HAs. Besides, the IBV HA0 cleavage loop might be structurally distinct from the A/H1 and A/H3 HA0 loops. While the latter two have been resolved (76, 77), an X-ray structure of IBV HA0 is still missing.

Since the clinical picture of IBV is similar to that of IAV (9), the high cleavability of IBV HA appears not linked to virulence. However, it assures shedding of infectious virus. Human-to-human transmissibility also requires optimal HA acid-stability, since this renders the virus more stable under mildly acidic conditions in the human URT or environment (25). For zoonotic IAVs, adaptation to the human host is associated with HA stabilization, reducing the HA fusion pH to 5.2-5.5 (29). This fits with the fusion pH values that we measured for IBV HA, i.e. 5.4 for the B/Victoria and 5.6 for the B/Yamagata lineage. Literature data for IBV are scarce but our values are in agreement with other reports (78, 79). The difference between the two lineages appears partially related to the B/Victoria lineage-specific N248 HA head glycan, positioned adjacent to the receptor binding site (7). Removing this *N*-glycan caused a small increase in the fusion pH threshold, pointing to an allosteric effect of this HA head on the fusion process, which is consistent with a role for receptor binding in fusion peptide dynamics (13).

For both IBV lineages, the HA was shown to exhibit a preference for 33°C which proved particularly pronounced for the B/Victoria lineage. Analysis of additional IBV strains could validate our hypothesis that, compared to the B/Yamagata lineage, B/Victoria HA might be even better adapted to the proximal airways, given its stricter 33°C dependence and lower fusion pH. Its more stable HA could perhaps explain higher prevalence of this lineage in children (9) which typically have a more acidic nasal pH (25). A preference for cooler temperature was also reported for the hemagglutinin-esterase-fusion (HEF) protein of influenza C virus, which mainly infects humans (80). We did not observe this temperature effect for human IAV HAs, and saw the opposite pattern for avian A/H7 HA. This leads us to hypothesize that fine-tuning of HA protein expression to fit the temperature of the host target organs could be another viral adaptation strategy, besides well-known mechanisms related to receptor use, polymerase activity or immune evasion (8). The temperature-sensitive expression of IBV HA is an intrinsic feature that does not require any other IBV proteins, hence it is unrelated to the reduced RNA synthesis seen with some temperature-sensitive IBV strains (81). As for the biochemical basis, for influenza C virus HEF protein, trimer formation and surface expression proved more efficient at 33°C than at 37°C (80). A similar temperature

effect may apply to IBV HA, since pseudoparticles carrying B/Vic HA contained much higher HA levels when produced at 33°C compared to 37°C. For IAV HA, a link exists between *N*-glycosylation and temperature sensitivity of the processes of HA folding or transport towards the cell membrane (74, 82-85). We therefore examined the role of the B/Victoria lineage-specific N248 glycan, however, removal of this HA head *N*-glycan did not change the dependence on 33°C.

Although our study was focused on the HA proteins of seasonal human IAV and IBV viruses, we also made an interesting observation for the HA of 1918 IAV. Its HA fusion pH (5.7) proved to be exceptionally high for a human IAV but identical to that of highly pathogenic avian A/H5N1 virus. This may help to explain the exceptional virulence of 1918 IAV, since IAVs with high HA fusion pH evade interferon control (86) and are more virulent in mice (87). It could also rationalize a mouse study in which the 1918 HA protein by itself generated a highly pathogenic phenotype when introduced in a contemporary backbone virus (48). Besides, we showed that TTSP activation is comparable for 1918 HA and other A/H1 HAs. Hence, the unique capacity of 1918 IAV to replicate in MDCK cells in the absence of trypsin (52, 55) seems not, or at least not entirely, explained by HA activation by TMPRSS4 or another TTSP expressed in MDCK cells. As proposed (55, 88), a role for the 1918 IAV neuraminidase is plausible.

To conclude, we demonstrated that the IBV HA protein combines broad and efficient activation capacity, favorable acid-stability and preference for the cooler temperature of the human URT. These distinct properties likely reflect host-adaptation resulting from sustained presence of this respiratory pathogen in the human population.

Materials and methods

Ethics statement

Lung tissue samples from eight different healthy donors were obtained under the approval of the ethical committee from the University Hospital Leuven (UZ Leuven Biobanking S51577). All patients were adult and provided written informed consent.

Cells, media and compounds

Calu-3 (ATCC #HTB-55), A549 (ATCC #CCL-185), 16HBE [a gift from P. Hoet (Leuven, Belgium)] and HeLa (ATCC #CCL-2) cells were grown in Minimum Essential Medium (MEM) supplemented with 10% fetal calf serum (FCS), 0.1 mM non-essential amino acids, 2 mM L-glutamine and 10 mM HEPES. HEK293T cells (Thermo Fisher Scientific #HCL4517) and Madin-Darby canine kidney (MDCK) cells, a gift from M. Matrosovich (Marburg, Germany), were grown in Dulbecco's modified Eagle's Medium supplemented with 10% FCS, 1 mM sodium pyruvate and 0.075% sodium bicarbonate. Medium with reduced (i.e. 0.2%) FCS content was used during protease expression and virus infection experiments. Except stated otherwise, all cell incubations were done at 37°C. The following compounds were purchased from Sigma-Aldrich: N-tosyl-L-phenylalanine chloromethyl ketone (TPCK)-treated trypsin, camostat, nafamostat, aprotinin and leupeptin. Chloromethylketone, E64-d and CA-074Me were from Enzo.

Viruses

The four human influenza virus strains and their abbreviations used in the text and figures are: A/Virginia/ATCC3/2009 (Virg09; A/H1N1 subtype; ATCC #VR-1737); A/HK/2/68 (HK68; A/H3N2 subtype) and B/Ned/537/05 (Ned05; B/Yamagata (B/Yam) lineage), both generously donated by R. Fouchier (Rotterdam, The Netherlands); and B/Malaysia/2506/04 (Mal04; B/Victoria (B/Vic) lineage; BEI resources #NR-12280). Viruses were expanded in 10-day old embryonated chicken eggs. For virus titration, a virus dilution series was added in quadruplo

to Calu-3 cells. At day 3 post infection (p.i.), virus positivity was assessed by immunostaining for viral nucleoprotein (NP) (see below). Virus titers were expressed as the 50% cell culture infective dose ($CCID_{50}$), calculated by the method of Reed and Muench (89).

Plasmids

The panel of thirty-five pcDNA3.1+/C-(K)DYK plasmids containing the coding sequences for the 18 TTSPs, 16 KLKs and furin (for accession numbers and Clone IDs, see S1 Table), was purchased from GenScript. The length of the ORFs was checked by PCR (S1 Fig). Expression of the different proteases was verified at 48 h post transfection of HEK293T cells, using dot blot assay. Cell lysates, prepared in RIPA buffer, were spotted onto a nitrocellulose membrane. The membrane was dried, blocked with 5% low fat milk powder in PBS, and incubated for 1 h with horseradish peroxidase (HRP)-conjugated anti-FLAG antibody (see full list of antibodies in S2 Table). The dots were detected using SuperSignal™ West Femto Maximum Sensitivity Substrate (Thermo Fisher Scientific) and the ChemiDoc XRS+ System (Bio-Rad).

The expression plasmid for canine TMPRSS4 was constructed by extracting total RNA from MDCK cells, followed by reverse transcription and high-fidelity PCR using primers extended with EcoRV and XbaI sites, to allow subcloning into the pCAGEN vector provided by C. Cepko (Boston, MA) via Addgene (plasmid #11160). A similar cloning procedure was used to prepare pCAGEN vectors with the HA and neuraminidase (NA) coding sequences from Virg09, HK68, Ned05 and Mal04, starting from allantoic virus stocks. These HA proteins were >99% identical to the following GenBank sequences published on NCBI (www.ncbi.nlm.nih.gov): AGI54750.1 (for Virg09); AFG71887.1 (for HK68); AGX16237.1 (for Ned05) and CY040449.1 (for Mal04). The coding sequences for the A/H1 HA from A/South Carolina/1/1918 (SC1918) (GenBank: AF117241.1) and the N248D-mutant form of Mal04 HA were ordered from IDT. The cDNAs for A/H5 HA (ACA47835.1) from A/duck/Hunan/795/2002 (Hunan02); and the A/H7 HA (EPI439507) and A/N9 NA (EPI439509) from A/Anhui/1/2013 (Anhui13) were purchased from Sino Biological. cDNAs were amplified by Platinum™ SuperFi™ PCR (Invitrogen) and subcloned in the pCAGEN expression vector as described above. A/H1 HA from A/PR/8/34

(PR8; Sequence ID: AYA81842.1) was subcloned into pCAGEN starting from a pVP-HA reverse genetics plasmid, kindly donated by Dr. M. Kim (Daejeon, Korea).

Protease gene expression analysis in cells and human lung tissue

Lung tissue samples from eight different healthy donors were used. Calu-3, 16HBE, A549 and HEK293T lysates were made from three different cell passages. Total RNA was extracted using the ReliaPrep™ RNA Cell Miniprep System (Promega) and 0.5 µg RNA was converted to cDNA with the High-Capacity cDNA Reverse Transcription Kit (Thermo Fisher Scientific). BRYT Green™ dye-based quantitative PCR (qPCR) was performed with the GoTaq™ qPCR Master Mix (Promega) and intron-spanning primer pairs (see S3 Table for a list of all primers), in an ABI 7500 Fast Real-Time PCR system (Applied Biosciences). Expression data were normalized to the geometric mean of three housekeeping genes (*GAPDH, HMBS, ACTB*) and analyzed using the $2^{-\Delta\Delta CT}$ method. All primers were checked for PCR efficiency and specificity by melt curve analysis. Microarray data for 108 healthy lung samples were obtained from GEO dataset GSE47460 (www.ncbi.nlm.nih.gov/geo) (90).

Western blot assay to monitor HA0 cleavage or HA protein expression

To assess HA0 cleavage in protease-expressing cells, HEK293T cells were seeded in growth medium at 300,000 cells per well in 12-well plates, and transfected with 0.5 µg pCAGEN-HA plasmid and 0.5 µg pcDNA3.1+/C-(K)DYK-protease plasmid, using Lipofectamine 2000 (Life Technologies). Four hours later, the growth medium was replaced by medium with 0.2% FCS and cells were further incubated at 37°C or 33°C (for B/Vic HA). At 48 h post transfection, the control well was exposed to 5 µg/ml TPCK-treated trypsin for 15 min at 37°C. Cells were then lysed in RIPA buffer supplemented with protease inhibitor cocktail (both from Thermo Fisher Scientific). The lysates were boiled for 5 min in 1X XT sample buffer containing 1X XT reducing agent (both from Bio-Rad) and resolved on 4-12% Bis-Tris XT Precast 26-well gels (Bio-Rad). Proteins were transferred to polyvinylidene difluoride membranes (Bio-Rad), blocked with 5% low fat milk powder, and probed for 1 h with primary antibody followed by 45 min with HRP-

conjugated secondary antibody. Clathrin served as the loading control (S2 Table for a list of all antibodies). The bands were detected and visualized as explained above for the dot blot assay.

To quantify HA protein expression at different temperatures, HEK293T or HeLa cells seeded in 12-well plates were transfected with pCAGEN-HA plasmid, incubated during 48 h at 33, 35, 37 or 39 °C, then exposed to exogenous trypsin when indicated. Cell extraction and western blot analysis were carried out as above.

Polykaryon assay to measure protease-mediated activation of HA or its fusion pH

The method was adapted from Vanderlinden *et al.* (91) to enable high-throughput format with high-content imaging. To perform the broad TTSP and KLK analysis, HeLa cells in black 96-well plates (20,000 cells per well) were reverse transfected with 50 ng pCAGEN-HA plasmid and 12.5 ng pcDNA3.1+/C-(K)DYK protease-plasmid (each condition in triplo) using Fugene 6 (Promega). After 24 h, the growth medium was replaced by medium with 0.2% FCS and cells were further incubated at 37°C or 33°C (for B/Vic HA). Another 24 h later, the control conditions (which received HA plasmid only) were exposed for 15 min to MEM containing 5 µg/ml TPCK-treated trypsin. After gentle washing with PBS plus Ca^{2+} and Mg^{2+} (PBS-CM), the cells were exposed for 15 min to PBS-CM that had been pH-adjusted with citric acid to the required pH (i.e. a pH 0.1 unit lower than the fusion pH of that HA). After this pulse, the acidic PBS-CM was removed and growth medium with 10% FCS was added to stop the reaction. The cells were allowed to fuse during 4 h at 37°C (33°C for B/Vic HA, or another temperature if specifically mentioned), then fixated with 4% paraformaldehyde in PBS (15 min), permeabilized with 0.1% Triton X-100 (15 min) and stained for 30 min with 2 µg/ml HCS Cell Mask stain (Life Technologies). The plates were imaged using the CellInsight™ CX5 High Content Imaging Platform (Thermo Scientific). Nine images were taken per well and polykaryons were identified and counted using the SpotDetector protocol of the HCI software.

To determine the fusion pH of the different HAs, HeLa cells were transfected with the pCAGEN-HA plasmids and HA0 was cleaved with exogenous trypsin as above. During the acidic pulse,

a range of acidic buffers was used having a pH between 4.9 to 6.0 with 0.1 increments. High-content imaging-based quantification of polykaryons was done as above. The fusion pH was defined as the pH at which the number of polykaryons was 50% of the maximum number (91).

Production of protease-activated HA pseudoparticles and transduction experiments

The method to produce fLuc-expressing retroviral vectors pseudotyped with a viral glycoprotein was previously described (92). In brief, HEK293T cells were transfected in 6-well plates, using calcium phosphate precipitation, with a mixture of plasmids encoding: MLV gag-pol (1.5 µg); an MLV vector coding for fLuc (3 µg); HA- and NA-expression plasmids (both 0.75 µg); plus the protease expression plasmids specified above (0.125 µg). The two additional expression vectors pCAGGS-HAT and pCAGGS-DESC1 were described before (72). At 16 h post transfection, the medium was replaced by medium with 2% FCS. At 48 h, the pseudoparticle-containing supernatants were harvested and clarified by centrifugation. To verify that all TTSP conditions contained a similar total number of pseudoparticles, they were subsequently exposed to trypsin. Namely, one half of the supernatant was left untreated and the other half was treated with 20 µg/ml trypsin for 15 min at 37°C, after which 20 µg/ml soybean trypsin inhibitor was added. To measure particle infectivity, HEK293T target cells were seeded in 96-well plates at a density of 20,000 cells per well. One day later, the cells were exposed to 100 µl virus stock, and 6 h later, fresh medium was added. To measure fLuc activity at day 3 post transduction, the cells were lysed for 10 min in 50 µl cold PBS with 0.5% Triton-X. The lysates were transferred to a white, opaque-walled 96-well plate and, after adding fLuc substrate (Beetle-Juice (PJK) kit), the signal was read in a microplate reader (Plate Chameleon V; Hidex) using MicroWin2000 software (version 4.44; Mikrotek Laborsysteme GmbH).

Virus replication following siRNA-mediated protease knockdown or exposure to trypsin

ON-TARGET*plus* siRNA SMARTpools targeting the thirty-five human proteases and a non-targeting (scrambled) control were ordered from Dharmacon (for catalogue numbers see S4 Table). siRNAs targeting canine TMPRSS4 and canine ST14/matriptase were custom-synthesized by IDT (see sequences provided in S4 Table). Cells suspended in a black 96-well plate (Calu-3: 35,000 cells per well, MDCK: 7,500 cells per well) were reverse transfected with 10 nM siRNA (each condition in quadruplo) using Lipofectamine RNAiMAX Transfection Reagent (Thermo Fisher Scientific). One day later, the transfection medium with 10% FCS was replaced by medium containing 0.2% FCS. Another 24 h later, the cells were infected with Virg09, HK68, Ned05 or Mal04 virus at a multiplicity of infection (MOI) of 100 $CCID_{50}$. At 72 h p.i., immunostaining for viral NP was performed. The cells were fixated for 5 min in 2% paraformaldehyde, permeabilized for 10 min with 0.1% Triton X-100, and blocked for 4 h in 1% bovine serum albumin (BSA). Next, the plates were stained overnight at 4°C with anti-NP antibody diluted in 1% BSA (for IAV: Hytest #3IN5 at 1/2000 and for IBV: Hytest #RIF17 at 1/2000). After washing in PBS containing 0.01% Tween, Alexa Fluor™ 488 secondary antibody (Invitrogen #A21424 at 1/500) was applied for 1 h at room temperature. Cell nuclei were stained with Hoechst (Thermo Fisher Scientific). The plates were imaged using the high-content platform specified above. Nine images per well were analyzed to determine the total (Hoechst) and infected (NP) cell numbers.

To measure their potential cytotoxic effects, the siRNAs were added to a parallel plate containing mock-infected cells. After five days incubation, cell viability was measured by the colorimetric MTS assay (CellTiter 96 AQ_{ueous} MTS Reagent from Promega) (93).

To quantify virus replication in the absence or presence of trypsin, the Calu-3 or MDCK cells were infected with virus as above, using infection medium with or without 2 µg/ml TPCK-treated trypsin, and 0.2% FCS. After 3 days incubation, the infection rate was determined by NP-staining and high-content imaging.

Data analysis

Unless stated otherwise, data shown are the mean ± SEM of three independent experiments. Graphpad Prism software (version 7.0) was used to analyze the data and construct the graphs. One-way ANOVA or Kruskal-Wallis with post hoc test for multiple comparisons was performed to compare groups as indicated in the figure legends. To compare two groups, the unpaired Student's t-test was used. *P*-values in the text and graphs are shown as: *≤ 0.05; **≤ 0.01, ***≤ 0.001; ****≤ 0.0001.

Acknowledgements

Part of this research work was performed using the 'Caps-It' research infrastructure (project ZW13-02) that was financially supported by the Hercules Foundation (FWO) and Rega Foundation, KU Leuven. The authors wish to thank John McDonough for assisting the GEO expression analysis; Dirk Daelemans for providing the high-content imaging infrastructure; and Wim van Dam for technical assistance.

References

1. World Health Organization. Influenza (seasonal) - Fact sheet No. 211 2018 Available from: http://www.who.int/mediacentre/factsheets/fs211/en/.

2. Iuliano AD, Roguski KM, Chang HH, Muscatello DJ, Palekar R, Tempia S, et al. Estimates of global seasonal influenza-associated respiratory mortality: a modelling study. Lancet. 2018;391(10127):1285-300.

3. Glezen PW, Schmier JK, Kuehn CM, Ryan KJ, Oxford J. The burden of influenza B: a structured literature review. Am J Public Health. 2013;103(3):e43-51.

4. Nielsen J, Vestergaard LS, Richter L, Schmid D, Bustos N, Asikainen T, et al. European all-cause excess and influenza-attributable mortality in the 2017/18 season: should the burden of influenza B be reconsidered? Clin Microbiol Infect. 2019 Feb 18. pii: S1198-743X(19)30058-8. doi: 10.1016/j.cmi.2019.02.011

5. Matias G, Taylor R, Haguinet F, Schuck-Paim C, Lustig R, Shinde V. Estimates of mortality attributable to influenza and RSV in the United States during 1997-2009 by influenza type or subtype, age, cause of death, and risk status. Influenza Other Respir Viruses. 2014;8(5):507-15.

6. Suzuki Y, Nei M. Origin and evolution of influenza virus hemagglutinin genes. Mol Biol Evol. 2002;19(4):501-9.

7. Vijaykrishna D, Holmes EC, Joseph U, Fourment M, Su YC, Halpin R, et al. The contrasting phylodynamics of human influenza B viruses. Elife. 2015;4:e05055.

8. Long JS, Mistry B, Haslam SM, Barclay WS. Host and viral determinants of influenza A virus species specificity. Nat Rev Microbiol. 2018;17:67-81.

9. Koutsakos M, Nguyen TH, Barclay WS, Kedzierska K. Knowns and unknowns of influenza B viruses. Future Microbiol. 2016;11(1):119-35.

10. Osterhaus AD, Rimmelzwaan GF, Martina BE, Bestebroer TM, Fouchier RA. Influenza B virus in seals. Science. 2000;288(5468):1051-3.

11. Byrd-Leotis L, Cummings RD, Steinhauer DA. The interplay between the host receptor and influenza virus hemagglutinin and neuraminidase. Int J Mol Sci. 2017;18(7):1541.

12. Cross KJ, Burleigh LM, Steinhauer DA. Mechanisms of cell entry by influenza virus. Expert Rev Mol Med. 2001;3(21):1-18.

13. Das DK, Govindan R, Nikic-Spiegel I, Krammer F, Lemke EA, Munro JB. Direct visualization of the conformational dynamics of single influenza hemagglutinin trimers. Cell. 2018;174:1-12.

14. Klenk HD, Rott R, Orlich M, Blödorn J. Activation of influenza A viruses by trypsin treatment. Virology. 1975;68(2):426-39.

15. Laporte M, Naesens L. Airway proteases: an emerging drug target for influenza and other respiratory virus infections. Curr Opin Virol. 2017;24:16-24.

16. Böttcher-Friebertshäuser E, Lu Y, Meyer D, Sielaff F, Steinmetzer T, Klenk HD, et al. Hemagglutinin activating host cell proteases provide promising drug targets for the treatment of influenza A and B virus infections. Vaccine. 2012;30(51):7374-80.

17. Böttcher-Friebertshäuser E, Garten W, Klenk HD. Activation of Viruses by Host Proteases. Springer; 2018.

18. Hatesuer B, Bertram S, Mehnert N, Bahgat MM, Nelson PS, Pöhlmann S, et al. Tmprss2 is essential for influenza H1N1 virus pathogenesis in mice. PLoS Pathog. 2013;9(12):e1003774.

19. Tarnow C, Engels G, Arendt A, Schwalm F, Sediri H, Preuss A, et al. TMPRSS2 is a host factor that is essential for pneumotropism and pathogenicity of H7N9 influenza A virus in mice. J Virol. 2014;88(9):4744-51.

20. Sakai K, Ami Y, Tahara M, Kubota T, Anraku M, Abe M, et al. The host protease TMPRSS2 plays a major role in in vivo replication of emerging H7N9 and seasonal influenza viruses. J Virol. 2014;88(10):5608-16.

21. Lambertz RLO, Gerhauser I, Nehlmeier I, Leist SR, Kollmus H, Pohlmann S, et al. Tmprss2 knock-out mice are resistant to H10 influenza A virus pathogenesis. J Gen Virol. 2019 Jul;100(7):1073-1078. doi: 10.1099/jgv.0.001274

22. Cheng Z, Zhou J, To KK, Chu H, Li C, Wang D, et al. Identification of TMPRSS2 as a susceptibility gene for severe 2009 pandemic A(H1N1) influenza and A(H7N9) influenza. J Infect Dis. 2015;212(8):1214-21.

23. Hamilton BS, Whittaker GR, Daniel S. Influenza virus-mediated membrane fusion: determinants of hemagglutinin fusogenic activity and experimental approaches for assessing virus fusion. Viruses. 2012;4(7):1144-68.

24. Sakai K, Ami Y, Nakajima N, Nakajima K, Kitazawa M, Anraku M, et al. TMPRSS2 independency for haemagglutinin cleavage in vivo differentiates influenza B virus from Iinfluenza A virus. Sci Rep. 2016;6:29430.

25. Russell CJ, Hu M, Okda FA. Influenza hemagglutinin protein stability, activation, and pandemic risk. Trends Microbiol. 2018;26(10):841-53.

26. Singanayagam A, Zambon M, Barclay W. Influenza virus with increased pH of HA activation has improved replication in cell culture but at the cost of infectivity in human airway epithelium. J Virol. 2019. DOI: 10.1128/JVI.00058-19.

27. Fischer H, Widdicombe JH. Mechanisms of acid and base secretion by the airway epithelium. J Membr Biol. 2006;211(3):139-50.

28. England RJ, Homer JJ, Knight LC, Ell SR. Nasal pH measurement: a reliable and repeatable parameter. Clinical otolaryngology and allied sciences. 1999;24(1):67-8.

29. Russier M, Yang G, Rehg JE, Wong SS, Mostafa HH, Fabrizio TP, et al. Molecular requirements for a pandemic influenza virus: An acid-stable hemagglutinin protein. Proc Natl Acad Sci U S A. 2016;113(6):1636-41.

30. Baumann J, Kouassi NM, Foni E, Klenk HD, Matrosovich M. H1N1 swine influenza viruses differ from avian precursors by a higher pH optimum of membrane fusion. J Virol. 2016;90(3):1569-77.

31. Imai M, Watanabe T, Hatta M, Das SC, Ozawa M, Shinya K, et al. Experimental adaptation of an influenza H5 HA confers respiratory droplet transmission to a reassortant H5 HA/H1N1 virus in ferrets. Nature. 2012;486(7403):420-8.

32. Linster M, van Boheemen S, de Graaf M, Schrauwen EJA, Lexmond P, Manz B, et al. Identification, characterization, and natural selection of mutations driving airborne transmission of A/H5N1 virus. Cell. 2014;157(2):329-39.

33. Lindemann J, Leiacker R, Rettinger G, Keck T. Nasal mucosal temperature during respiration. Clinical otolaryngology and allied sciences. 2002;27(3):135-9.

34. McFadden ER, Jr., Pichurko BM, Bowman HF, Ingenito E, Burns S, Dowling N, et al. Thermal mapping of the airways in humans. J Appl Physiol 1985;58(2):564-70.

35. Massin P, van der Werf S, Naffakh N. Residue 627 of PB2 is a determinant of cold sensitivity in RNA replication of avian influenza viruses. J Virol. 2001;75(11):5398-404.

36. Aggarwal S, Dewhurst S, Takimoto T, Kim B. Biochemical impact of the host adaptation-associated PB2 E627K mutation on the temperature-dependent RNA synthesis kinetics of influenza A virus polymerase complex. J Biol Chem. 2011;286(40):34504-13.

37. Scull MA, Gillim-Ross L, Santos C, Roberts KL, Bordonali E, Subbarao K, et al. Avian Influenza virus glycoproteins restrict virus replication and spread through human airway epithelium at temperatures of the proximal airways. PLoS Pathog. 2009;5(5):e1000424.

38. Ohler A, Becker-Pauly C. TMPRSS4 is a type II transmembrane serine protease involved in cancer and viral infections. Biol Chem. 2012;393(9):907-14.

39. Kalinska M, Meyer-Hoffert U, Kantyka T, Potempa J. Kallikreins - The melting pot of activity and function. Biochimie. 2016;122:270-82.

40. Garten HD, Garten W. Host cell proteases controlling virus pathogenicity. Trends in Microbiology. 1994;2(2):39-43.

41. Thomas G. Furin at the cutting edge: From protein traffic to embryogenesis and disease. Nat Rev Mol Cell Bio. 2002;3(10):753-66.

42. Bertram S, Glowacka I, Blazejewska P, Soilleux E, Allen P, Danisch S, et al. TMPRSS2 and TMPRSS4 facilitate trypsin-independent spread of influenza virus in Caco-2 cells. J Virol. 2010;84(19):10016-25.

43. Floyd LD, Ragains JR, J.J. S, Harrison SC, van Oijen AM. Single-particle kinetics of influenza virus membrane fusion. Proc Natl Acad Sci U S A. 2008;105(40):15382–7.

44. Ivanovic T, Choi JL, Whelan SP, van Oijen AM, Harrison SC. Influenza-virus membrane fusion by cooperative fold-back of stochastically induced hemagglutinin intermediates. Elife. 2013;2:e00333.

45. Galloway SE, Reed ML, Russell CJ, Steinhauer DA. Influenza HA subtypes demonstrate divergent phenotypes for cleavage activation and pH of fusion: implications for host range and adaptation. PLoS Pathog. 2013;9(2):e1003151.

46. Gamblin SJ, Skehel JJ. Influenza hemagglutinin and neuraminidase membrane glycoproteins. J Biol Chem. 2010;285(37):28403-9.

47. Kobasa D, Takada A, Shinya K, Hatta M, Halfmann P, Theriault S, et al. Enhanced virulence of influenza A viruses with the haemagglutinin of the 1918 pandemic virus. Nature. 2004;431(7009):703-7.

48. Watanabe T, Tisoncik-Go J, Tchitchek N, Watanabe S, Benecke AG, Katze MG, et al. 1918 Influenza virus hemagglutinin (HA) and the viral RNA polymerase complex enhance viral pathogenicity, but only HA induces aberrant host responses in mice. J Virol. 2013;87(9):5239-54.

49. Taubenberger JK, Morens DM. 1918 influenza: the mother of all pandemics. Emerg Infect Dis. 2006;12(1):15-22.

50. Short KR, Kedzierska K, van de Sandt CE. Back to the future: lessons learned from the 1918 influenza pandemic. Front Cell Infect Microbiol. 2018;8:343.

51. Quan C, Shi W, Yang Y, Yang Y, Liu X, Xu W, et al. New threats from H7N9 influenza virus: spread and evolution of high- and low-pathogenicity variants with high genomic diversity in wave five. J Virol. 2018;92(11):e00301-18.

52. Chaipan C, Kobasa D, Bertram S, Glowacka I, Steffen I, Tsegaye TS, et al. Proteolytic activation of the 1918 influenza virus hemagglutinin. J Virol. 2009;83(7):3200-11.

53. Zhou Y, Vedantham P, Lu K, Agudelo J, Carrion R, Jr., Nunneley JW, et al. Protease inhibitors targeting coronavirus and filovirus entry. Antiviral Res. 2015;116:76-84.

54. Noma K, Kiyotani K, Kouchi H, Fujii Y, Egi Y, Tanaka K, et al. Endogenous protease-dependent replication of human influenza viruses in two MDCK cell lines. Arch Virol. 1998;143(10):1893-909.

55. Tumpey TM, Basler CF, Aguilar PV, Zeng H, Solorzano A, Swayne DE, et al. Characterization of the reconstructed 1918 Spanish influenza pandemic virus. Science. 2005;310(5745):77-80.

56. Godiksen S, Selzer-Plon J, Pedersen ED, Abell K, Rasmussen HB, Szabo R, et al. Hepatocyte growth factor activator inhibitor-1 has a complex subcellular itinerary. Biochem J. 2008;413(2):251-9.

57. Baron J, Tarnow C, Mayoli-Nussle D, Schilling E, Meyer D, Hammami M, et al. Matriptase, HAT, and TMPRSS2 activate the hemagglutinin of H9N2 influenza A viruses. J Virol. 2013;87(3):1811-20.

58. Lugovtsev VY, Melnyk D, Weir JP. Heterogeneity of the MDCK cell line and its applicability for influenza virus research. Plos One. 2013;8(9):e75014.

59. Hamilton BS, Gludish DW, Whittaker GR. Cleavage activation of the human-adapted influenza virus subtypes by matriptase reveals both subtype and strain specificities. J Virol. 2012;86(19):10579-86.

60. Beaulieu A, Gravel E, Cloutier A, Marois I, Colombo E, Desilets A, et al. Matriptase proteolytically activates influenza virus and promotes multicycle replication in the human airway epithelium. J Virol. 2013;87(8):4237-51.

61. McShane D, Davies JC, Davies MG, Bush A, Geddes DM, Alton EW. Airway surface pH in subjects with cystic fibrosis. Eur Respir J. 2003;21(1):37-42.

62. Russell CJ. Acid-induced membrane fusion by the hemagglutinin protein and its role in influenza virus biology. Curr Top Microbiol Immunol. 2014;385:93-116.

63. Zaraket H, Bridges OA, Russell CJ. The pH of activation of the hemagglutinin protein regulates H5N1 influenza virus replication and pathogenesis in mice. J Virol. 2013;87(9):4826-34.

64. Zaraket H, Baranovich T, Kaplan BS, Carter R, Song MS, Paulson JC, et al. Mammalian adaptation of influenza A(H7N9) virus is limited by a narrow genetic bottleneck. Nat Commun. 2015;6:6553.

65. Mittal A, Shangguan T, Bentz J. Measuring pKa of activation and pKi of inactivation for influenza hemagglutinin from kinetics of membrane fusion of virions and of HA expressing cells. Biophys J. 2002;83(5):2652–66.

66. Prinzinger R, Preßmar A, Schleucher E. Body temperature in birds. Comp Biochem Phys. 1991;99(4):499-506.

67. An Y, Cipollo JF. An unbiased approach for analysis of protein glycosylation and application to influenza vaccine hemagglutinin. Anal Biochem. 2011;415(1):67-80.

68. Ni F, Kondrashkina E, Wang Q. Structural basis for the divergent evolution of influenza B virus hemagglutinin. Virology. 2013;446(1-2):112-22.

69. Hamilton BS, Whittaker GR. Cleavage activation of human-adapted influenza virus subtypes by kallikrein-related peptidases 5 and 12. J Biol Chem. 2013;288(24):17399-407.

70. Magnen M, Elsasser BM, Zbodakova O, Kasparek P, Gueugnon F, Petit-Courty A, et al. Kallikrein-related peptidase 5 and seasonal influenza viruses, limitations of the experimental models for activating proteases. Biol Chem. 2018;399(9):1053-64.

71. Garten W, Braden C, Arendt A, Peitsch C, Baron J, Lu Y, et al. Influenza virus activating host proteases: identification, localization and inhibitors as potential therapeutics. Eur J Cell Biol. 2015;94(7-9):375-83.

72. Zmora P, Blazejewska P, Moldenhauer AS, Welsch K, Nehlmeier I, Wu Q, et al. DESC1 and MSPL activate influenza A viruses and emerging coronaviruses for host cell entry. J Virol. 2014;88(20):12087-97.

73. Zhirnov OP, Manykin AA, Rossman JS, Klenk HD. Intravirion cohesion of matrix protein M1 with ribonucleocapsid is a prerequisite of influenza virus infectivity. Virology. 2016;492:187-96.

74. Hebert DN, Zhang JX, Chen W, Foellmer B, Helenius A. The number and location of glycans on influenza hemagglutinin determine folding and association with calnexin and calreticulin. J Cell Biol. 1997;139(3):613-23.

75. Sakai K, Sekizuka T, Ami Y, Nakajima N, Kitazawa M, Sato Y, et al. A mutant H3N2 influenza virus uses an alternative activation mechanism in TMPRSS2 knockout mice by loss of an oligosaccharide in the hemagglutinin stalk region. J Virol. 2015;89(9):5154-8.

76. Chen J, Lee KH, Steinhauer DA, Stevens DJ, Skehel JJ, Wiley DC. Structure of the hemagglutinin precursor cleavage site, a determinant of influenza pathogenicity and the origin of the labile conformation. Cell. 1998;95(3):409-17.

77. Stevens J, Corper AL, Basler CF, Taubenberger JK, Palese P, Wilson IA. Structure of the uncleaved human H1 hemagglutinin from the extinct 1918 influenza virus. Science. 2004;303(5665):1866-70.

78. Brassard DL, Lamb RA. Expression of influenza B virus hemagglutinin containing multibasic residue cleavage sites. Virology. 1997;236(2):234-48.

79. Nakowitsch S, Waltenberger AM, Wressnigg N, Ferstl N, Triendl A, Kiefmann B, et al. Egg- or cell culture-derived hemagglutinin mutations impair virus stability and antigen content of inactivated influenza vaccines. Biotechnol J. 2014;9(3):405-14.

80. Takashita E, Muraki Y, Sugawara K, Asao H, Nishimura H, Suzuki K, et al. Intrinsic temperature sensitivity of influenza C virus hemagglutinin-esterase-fusion protein. J Virol. 2012;86(23):13108-11.

81. Chen Z, Aspelund A, Kemble G, Jin H. Molecular studies of temperature-sensitive replication of the cold-adapted B/Ann Arbor/1/66, the master donor virus for live attenuated influenza FluMist vaccines. Virology. 2008;380(2):354-62.

82. Ueda M, Sugiura A. Physiological characterization of influenza virus temperature-sensitive mutants defective in the haemagglutinin gene. J Gen Virol. 1984;65 1889-97.

83. Schuy W, Will C, Kuroda K, Scholtissek C, Garten W, Klenk HD. Mutations blocking the transport of the influenza virus hemagglutinin between the rough endoplasmic reticulum and the Golgi apparatus. EMBO J. 1986;5(11):2831-6.

84. Gallagher PJ, Henneberry JM, Sambrook JF, Gething MJ. Glycosylation requirements for intracellular transport and function of the hemagglutinin of influenza virus. J Virol. 1992;66(12):7136-45.

85. Roberts PC, Garten W, Klenk HD. Role of conserved glycosylation sites in maturation and transport of influenza A virus hemagglutinin. J Virol. 1993;67(6):3048-60.

86. Gerlach T, Hensen L, Matrosovich T, Bergmann J, Winkler M, Peteranderl C, et al. pH Optimum of hemagglutinin-mediated membrane fusion determines sensitivity of influenza A viruses to the interferon-induced antiviral state and IFITMs. J Virol. 2017;91(11):1-16.

87. Koerner I, Matrosovich MN, Haller O, Staeheli P, Kochs G. Altered receptor specificity and fusion activity of the haemagglutinin contribute to high virulence of a mouse-adapted influenza A virus. J Gen Virol. 2012;93(Pt 5):970-9.

88. Takahashi T, Kurebayashi Y, Ikeya K, Mizuno T, Fukushima K, Kawamoto H, et al. The low-pH stability discovered in neuraminidase of 1918 pandemic influenza A virus enhances virus replication. Plos One. 2010;5(12):e15556.

89. Reed LJ, Muench H. A simple method of estimating fifty per cent endpoints. Am J Epidemiol. 1938;27(3):493-7.

90. McDonough JE, Kaminski N, Thienpont B, Hogg JC, Vanaudenaerde BM, Wuyts WA. Gene correlation network analysis to identify regulatory factors in idiopathic pulmonary fibrosis. Thorax. 2019;74(2):132-40.

91. Vanderlinden E, Göktas F, Cesur Z, Froeyen M, Reed ML, Russell CJ, et al. Novel inhibitors of influenza virus fusion: structure-activity relationship and interaction with the viral hemagglutinin. J Virol. 2010;84(9):4277-88.

92. Simmons G, Reeves JD, Grogan CC, Vandenberghe LH, Baribaud F, Whitbeck JC, et al. DC-SIGN and DC-SIGNR bind Ebola glycoproteins and enhance infection of macrophages and endothelial Cells. Virology. 2003;305(1):115-23.

93. Vrijens P, Noppen S, Boogaerts T, Vanstreels E, Ronca R, Chiodelli P, et al. Influenza virus entry via the GM3 ganglioside-mediated platelet-derived growth factor receptor beta signalling pathway. J Gen Virol. 2019;100(4):583-601.

Figure titles and legends

Fig 1. Human lung tissue and airway epithelial cell lines are rich in TTSP and KLK enzymes.

(A) *TTSP* and (B) *KLK* transcript levels in healthy human lung, measured by RT-qPCR on samples from eight different donors (left), or retrieved from the NCBI GEO database (GEO dataset GSE47460) (right). Individual data points (in black) ± SEM (in pink). °No data available. (C, D) Transcript levels in human airway epithelial Calu-3, 16HBE and A549 cells, and human embryonic kidney HEK293T cells. (E) Heatmap visualizing the mRNA expression levels in panels A-D, ranging from no expression (0) to high expression (4).

Fig 2. IBV HA0 is efficiently cleaved by a broad range of TTSPs.

(A) Experiment set-up. HEK293T cells were transfected with two plasmids, one encoding IAV or IBV HA and one encoding the indicated TTSP, KLK or furin. The HA cleavage state was determined at 48 h post transfection. (B) Representative western blots showing the bands of uncleaved HA0 and cleaved HA1 or HA2. The trypsin controls (second lanes on each row), consisted of cells transfected with HA and a protease-lacking empty plasmid, and exposed to trypsin for 15 min just before cell extraction. (C) Quantitative data for TTSP- and KLK-mediated HA0 cleavage. For each HA, the intensity of the HA1 or HA2 band was normalized to clathrin and the % cleaved HA (mean ± SEM; N=3) was expressed relative to the trypsin control. *P*-value *versus* no trypsin: *≤ 0.05; **≤ 0.01; ***≤ 0.001; ****≤ 0.0001 (ordinary one-way ANOVA, followed by Dunnett's test).

Fig 3. TTSP cleavage generates fusion-competent HA proteins.

(A) Experiment set-up. HeLa cells expressing IAV or IBV HA plus a TTSP or KLK protease were exposed to an acidic buffer 0.1 units below the HA fusion pH. (B) Microscopic images showing polykaryon formation in cells expressing IBV (B/Yam) HA. The yellow contours show the polykaryons identified by high-content imaging software. The trypsin control (third

photograph) received an empty (i.e. protease-lacking) plasmid and underwent HA activation by 15 min exposure to trypsin just before the acidic pulse. (C) Quantitative data for TTSP- and KLK-mediated polykaryon formation. The number of polykaryons is expressed relative to the trypsin control. Data are the mean ± SEM (N=3 with triplicate read-outs). *P*-value *versus* no trypsin: *≤ 0.05; ***≤ 0.001; ****≤ 0.0001 (ordinary one-way ANOVA, followed by Dunnett's test).

Fig 4. Pseudoparticles carrying IBV HA are efficiently activated by different TTSPs.

(A) Experiment set-up. HEK293T producer cells were transfected with plasmids encoding the HA and NA from IAV or IBV, MLV-backbone, MLV-luciferase reporter and a TTSP enzyme. The produced pseudoparticles were left untreated (to assess TTSP-induced infectivity), or secondarily treated with trypsin (to measure total particle infectivity). After transducing HEK293T target cells, luminescence was measured at day 3 day p.i. (B, C) Transduction efficiency (relative to the trypsin control) of TTSP-activated pseudoparticles tested as such (in color) or after additional trypsin treatment (in white). Data are the mean ± SEM (N=3 with triplicate read-outs). *P*-value *versus* no trypsin: *≤ 0.05; ***≤ 0.001; ****≤ 0.0001 (Kruskall-Wallis, followed by Dunnett's test).

Fig 5. TMPRSS2 is a crucial protease for replication of IAV but not IBV.

(A) Experiment set-up. Calu-3 cells were transfected with TTSP- or KLK-targeting siRNA and infected with IAV or IBV. The % infected cells was quantified by high-content imaging of NP. (B) Impact of protease knockdown on cell viability (grey bars) or virus growth (colored bars), expressed relative to the condition receiving no siRNA. Data are the mean ± SEM (N=3 with four replicates). *P*-value *versus* scrambled siRNA: *≤ 0.05; ***≤ 0.001; ****≤ 0.0001 (ordinary one-way ANOVA, followed by Dunnett's test). (C) TMPRSS2 knockdown markedly reduces IAV but not IBV replication, as shown by NP-staining. (D) IBV infection in Calu-3 cells receiving combinations of siRNAs.

Fig 6. MDCK cells contain high levels of HA-activating TMPRSS4.

(A, B) IAV or IBV replication in MDCK cells in the presence or absence of trypsin. Panel A: % infected cells at day 3 p.i., quantified by high-content imaging of NP. Mean ± SEM of two experiments performed in quadruplo. Panel B: HA0 cleavage state at day 3 p.i. in cells receiving 0 or 10 µM camostat. (C) Expression of TTSP and KLK proteases in MDCK cells (normalized to canine *GAPDH* and *HMBS*). °Undetermined; *no data (no dog mRNA sequence was available to design primers). (D) Canine TMPRSS4 activates the HAs of IAV and IBV. Western blot, from left to right: HA0 band in HEK293T cells receiving no protease, exogenous trypsin, or the canine TMPRSS4 plasmid at three different concentrations. Under each lane, the HA0 band intensity is given (normalized to clathrin and expressed relative to the no trypsin condition). Photographs: polykaryon formation in HeLa cells undergoing co-expression of HA and canine TMPRSS4. (E, F) Effect of TMPRSS4 and/or ST14/matriptase knockdown in MDCK cells. Panel E: mRNA levels at 24 h post siRNA transfection, normalized to canine *HMBS* and *GAPDH* and shown as the fold change *versus* untransfected control. Panel F: siRNA-transfected cells were infected with B/Yam or B/Vic virus, and at day 3 p.i., HA0 cleavage state was determined by western blot and virus infection was assessed by high-content imaging of NP.

Fig 7. IBV HA exhibits a similar fusion pH as human-adapted IAV HAs.

(A) Experiment set-up. HA-expressing HeLa cells were activated with exogenous trypsin, then exposed to a range of acidic buffers to induce cell-cell fusion. (B, C, D, E) Curves showing the number of polykaryons in function of the pH applied to trigger HA. Data are the mean ± SEM of two independent experiments, each performed in triplicate. The insets show the fusion pH values, defined as the pH at which the number of polykaryons was 50% of the maximum number.

Fig 8. IBV HA prefers a temperature of 33°C for protein expression, explaining temperature-restricted fusion of B/Vic HA.

(A) HeLa cells were transfected with the indicated HA plasmids and incubated during 48 h at different temperatures. The graphs show quantitative western blot data for HA0 band intensity, normalized to clathrin, and expressed relative to the HA0 band seen at 33°C. Data are the mean ± SEM (N=3). *P*-values: *< 0.05, **< 0.01, ****≤ 0.0001 (ordinary one-way ANOVA, followed by Dunnett's test). (B, C, D) Polykaryon formation in IBV HA-transfected HeLa cells exposed to different temperatures during the stages of HA expression (starting 24 h post transfection) or cell-cell fusion. Panel B: fusion induced by a pH 5.0 buffer. Panel C and panel D: number of polykaryons in function of pH, after HA expression at 33°C (C) or 37°C (D). The western blots show the corresponding HA levels after trypsin activation. (E) B/Vic (Mal04) pseudoparticles were produced at 33°C or 37°C, activated with trypsin, and transduced into HEK293T cells at 33°C or 37°C. Left: luminescence readout. Right: HA levels in released pseudoparticles collected by ultracentrifugation (top) and in HEK293T producer cells (bottom).

Supporting information

S1 Table. Overview of the thirty-five pcDNA3.1+/C-(K)DYK expression vectors used.

S2 Table. Antibodies for western blot detection of IAV or IBV HA and dot blot detection of FLAG-tagged proteases.

S3 Table. Primers for RT-qPCR quantification of human and canine *TTSP* or *KLK* mRNA in cells and lung tissue.

S4 Table. Human and canine siRNAs used for protease knockdown studies in Calu-3 and MDCK cells.

S5 Table. Antiviral activity of protease inhibitors and influenza virus inhibitors in Calu-3 cells infected with IAV or IBV.

S1 Fig. PCR control and protein expression levels for the TTSP- and KLK-expression plasmids. (A) The correct length of the ORFs was checked by PCR using a CMV promoter-directed forward primer and flag/DYK-directed reverse primer. (B) Successful protein expression after plasmid transfection in HEK293T cells was checked by anti-flag dot blot assay. °Untransfected cell control; *cells transfected with empty vector. (C) Quantification of the dots shown in panel B; dot intensities were calculated relative to the TMPRSS2 dot, set at 100%.The numbers correspond to the plasmid numbers shown in S1 Table.

S2 Fig. Transduction efficiency of A/H1N1 pseudoparticles and their HA cleavage state. H1N1 influenza pseudoparticles treated with trypsin were used to transduce HEK293T cells, luminescence was measured 3 days p.i. To assess Gag incorporation and HA cleavage status of the pseudoparticles, particles were purified by ultracentrifugation through a 20% sucrose cushion. The pellets were resuspended in SDS-PAGE sample buffer and analyzed by western blot. MLV-Gag was detected using an anti-MLV-p30 mouse antibody (Acris).

S3 Fig. Trypsin-independent replication of IAV and IBV in Calu-3 cells.
At day 3 p.i., virus was quantified by immunostaining for viral NP followed by high content imaging. The bar graph shows the mean ± SEM ; ns: not significant (*P*-value > 0.1 by unpaired t-test comparing the condition in the presence *versus* absence of trypsin).

S4 Fig. Optimization of siRNA transfection in Calu-3 cells. Calu-3 cells were transfected with different amounts of siGLO Green Transfection Indicator (Dharmacon) using two different approaches. (A) cells were plated on day 1 and transfection complexes were added on day 2 (forward transfection). (B) cells and transfection mixes were added at the same time (reverse transfection). Cells were imaged by fluorescence microscopy at 24 h post transfection. (C) Analysis of *GAPDH* and *TMPRSS2* mRNA knockdown at 24 h post siRNA reverse transfection. Relative differences were calculated as the fold change *versus* the untransfected control sample (no siRNA).

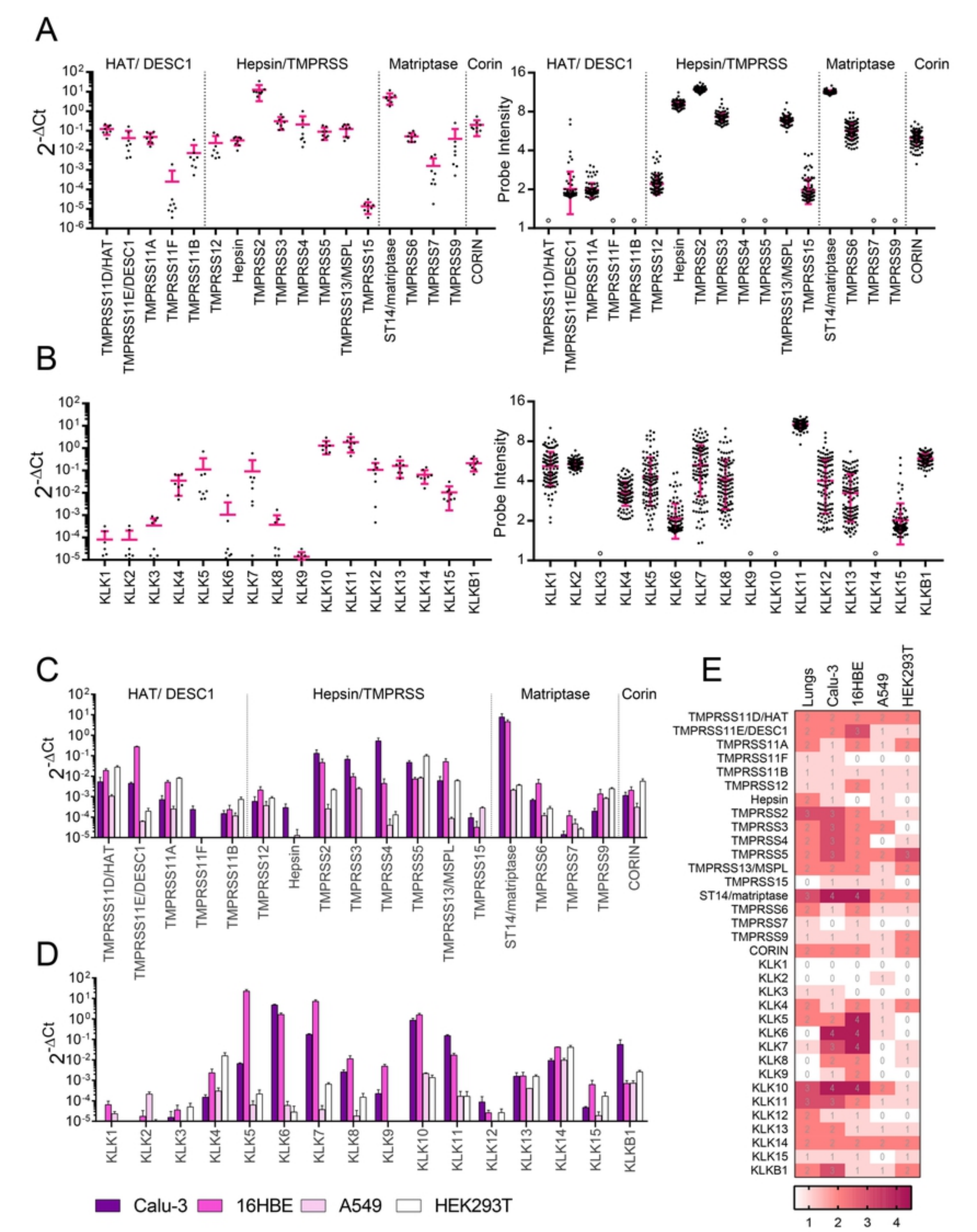
A
HAT/ DESC1
Hepsin/TMPRSS
Matriptase
Corin
2-ΔCt
Probe Intensity
TMPRSS11D/HAT
TMPRSS11E/DESC1
TMPRSS11A
TMPRSS11F
TMPRSS11B
TMPRSS12
Hepsin
TMPRSS2
TMPRSS3
TMPRSS4
TMPRSS5
TMPRSS13/MSPL
TMPRSS15
ST14/matriptase
TMPRSS6
TMPRSS7
TMPRSS9
CORIN
B
KLK1
KLK2
KLK3
KLK4
KLK5
KLK6
KLK7
KLK8
KLK9
KLK10
KLK11
KLK12
KLK13
KLK14
KLK15
KLKB1
C
D
Calu-3
16HBE
A549
HEK293T
E
Lungs
Calu-3
16HBE
A549
HEK293T

Fig 1

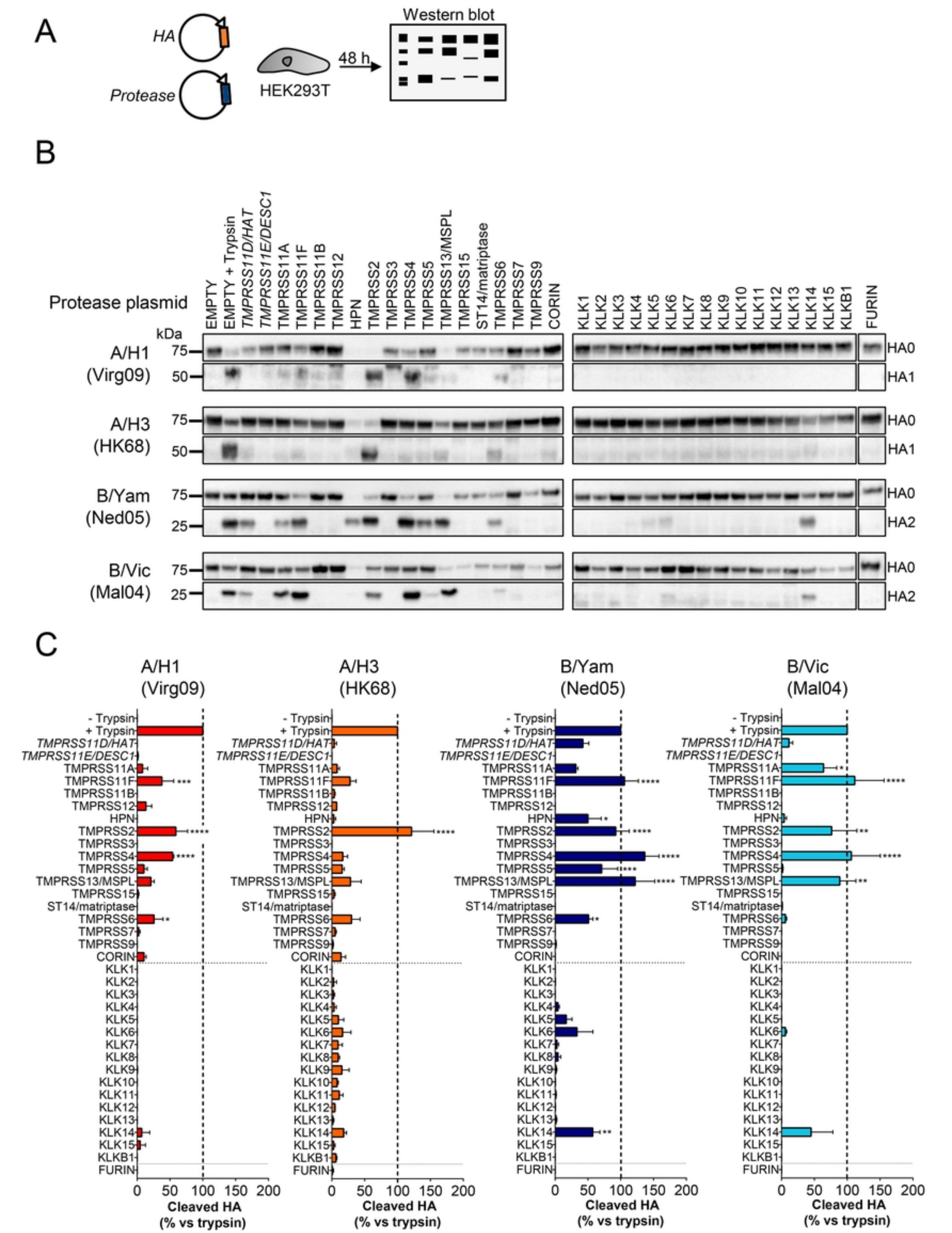
A
HA
Protease
HEK293T
48 h
Western blot
B
Protease plasmid
EMPTY
EMPTY + Trypsin
TMPRSS11D/HAT
TMPRSS11E/DESC1
TMPRSS11A
TMPRSS11F
TMPRSS11B
TMPRSS12
HPN
TMPRSS2
TMPRSS3
TMPRSS4
TMPRSS5
TMPRSS13/MSPL
TMPRSS15
ST14/matriptase
TMPRSS6
TMPRSS7
TMPRSS9
CORIN
KLK1
KLK2
KLK3
KLK4
KLK5
KLK6
KLK7
KLK8
KLK9
KLK10
KLK11
KLK12
KLK13
KLK14
KLK15
KLKB1
FURIN
kDa
A/H1 (Virg09)
A/H3 (HK68)
B/Yam (Ned05)
B/Vic (Mal04)
75
50
25
HA0
HA1
HA2
C
A/H1 (Virg09)
A/H3 (HK68)
B/Yam (Ned05)
B/Vic (Mal04)
- Trypsin
+ Trypsin
Cleaved HA (% vs trypsin)
0
50
100
150
200

Fig 2

A

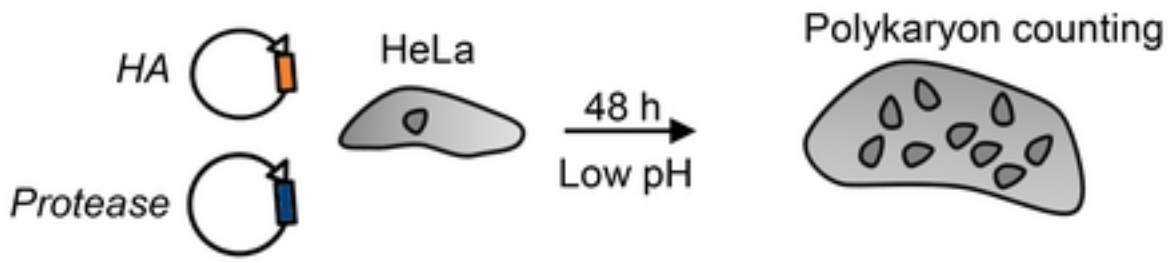
HA
Protease
HeLa
48 h
Low pH
Polykaryon counting

B

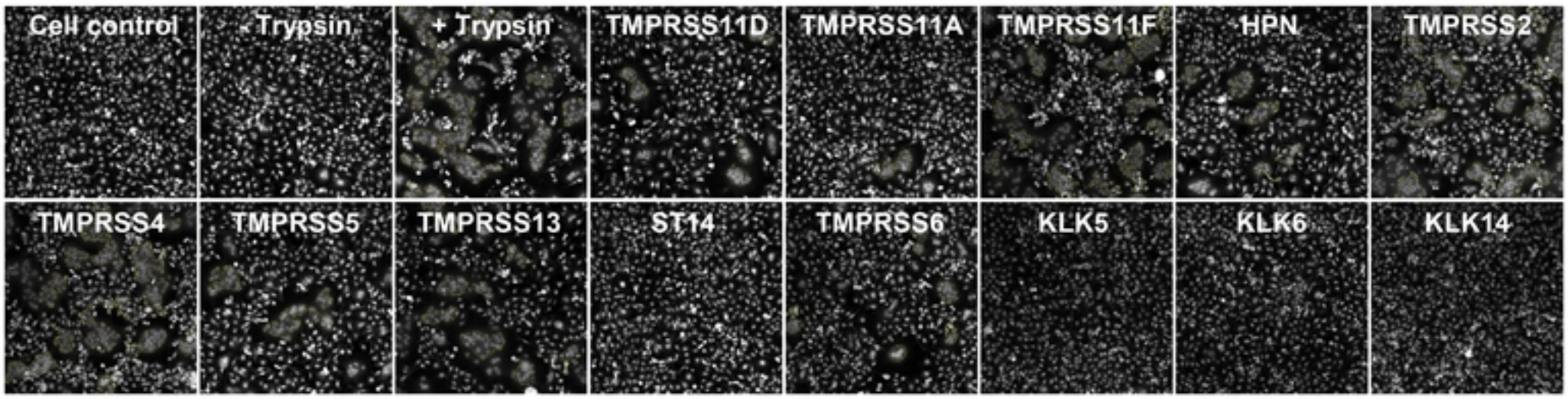
Cell control
- Trypsin
+ Trypsin
TMPRSS11D
TMPRSS11A
TMPRSS11F
HPN
TMPRSS2
TMPRSS4
TMPRSS5
TMPRSS13
ST14
TMPRSS6
KLK5
KLK6
KLK14

C

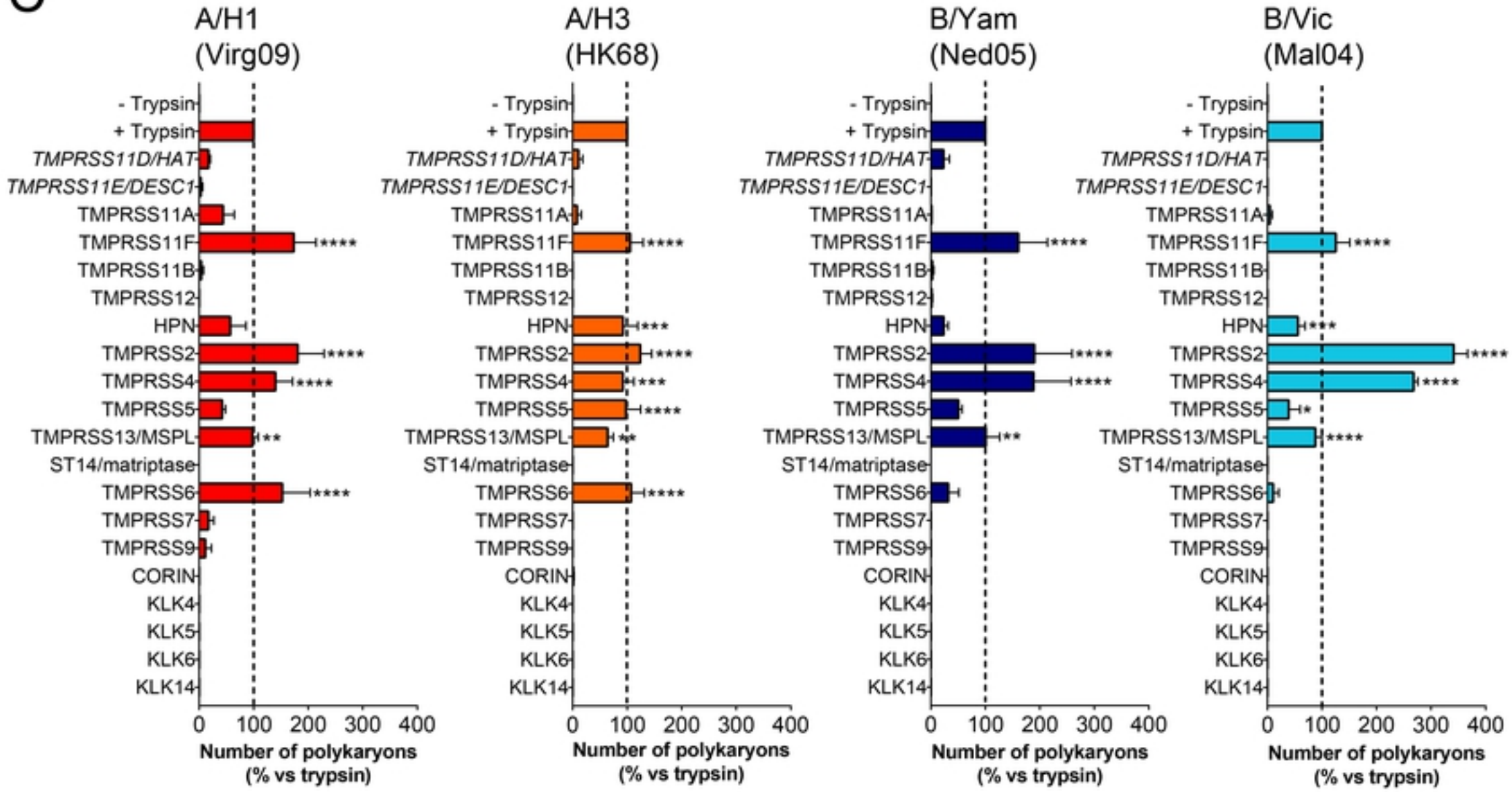
A/H1 (Virg09)
A/H3 (HK68)
B/Yam (Ned05)
B/Vic (Mal04)
- Trypsin
+ Trypsin
TMPRSS11D/HAT
TMPRSS11E/DESC1
TMPRSS11A
TMPRSS11F
TMPRSS11B
TMPRSS12
HPN
TMPRSS2
TMPRSS4
TMPRSS5
TMPRSS13/MSPL
ST14/matriptase
TMPRSS6
TMPRSS7
TMPRSS9
CORIN
KLK4
KLK5
KLK6
KLK14
0 100 200 300 400
Number of polykaryons (% vs trypsin)

Fig 3

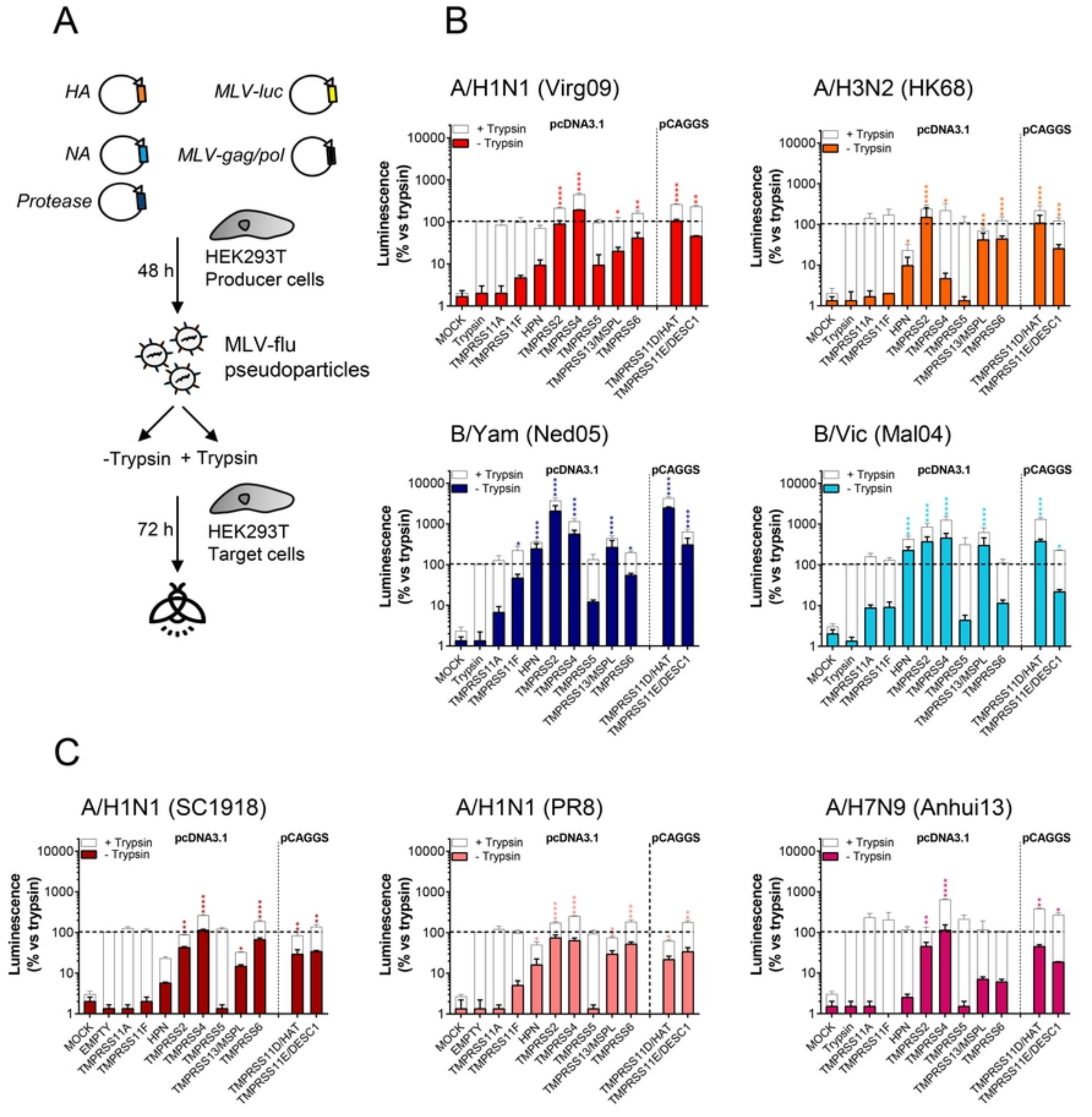
A
HA
MLV-luc
NA
MLV-gag/pol
Protease
48 h
HEK293T
Producer cells
MLV-flu
pseudoparticles
-Trypsin + Trypsin
72 h
HEK293T
Target cells
B
A/H1N1 (Virg09)
A/H3N2 (HK68)
B/Yam (Ned05)
B/Vic (Mal04)
+ Trypsin
- Trypsin
pcDNA3.1
pCAGGS
Luminescence
(% vs trypsin)
MOCK
Trypsin
TMPRSS11A
TMPRSS11F
HPN
TMPRSS2
TMPRSS4
TMPRSS5
TMPRSS13/MSPL
TMPRSS6
TMPRSS11D/HAT
TMPRSS11E/DESC1
C
A/H1N1 (SC1918)
A/H1N1 (PR8)
A/H7N9 (Anhui13)
EMPTY

Fig 4

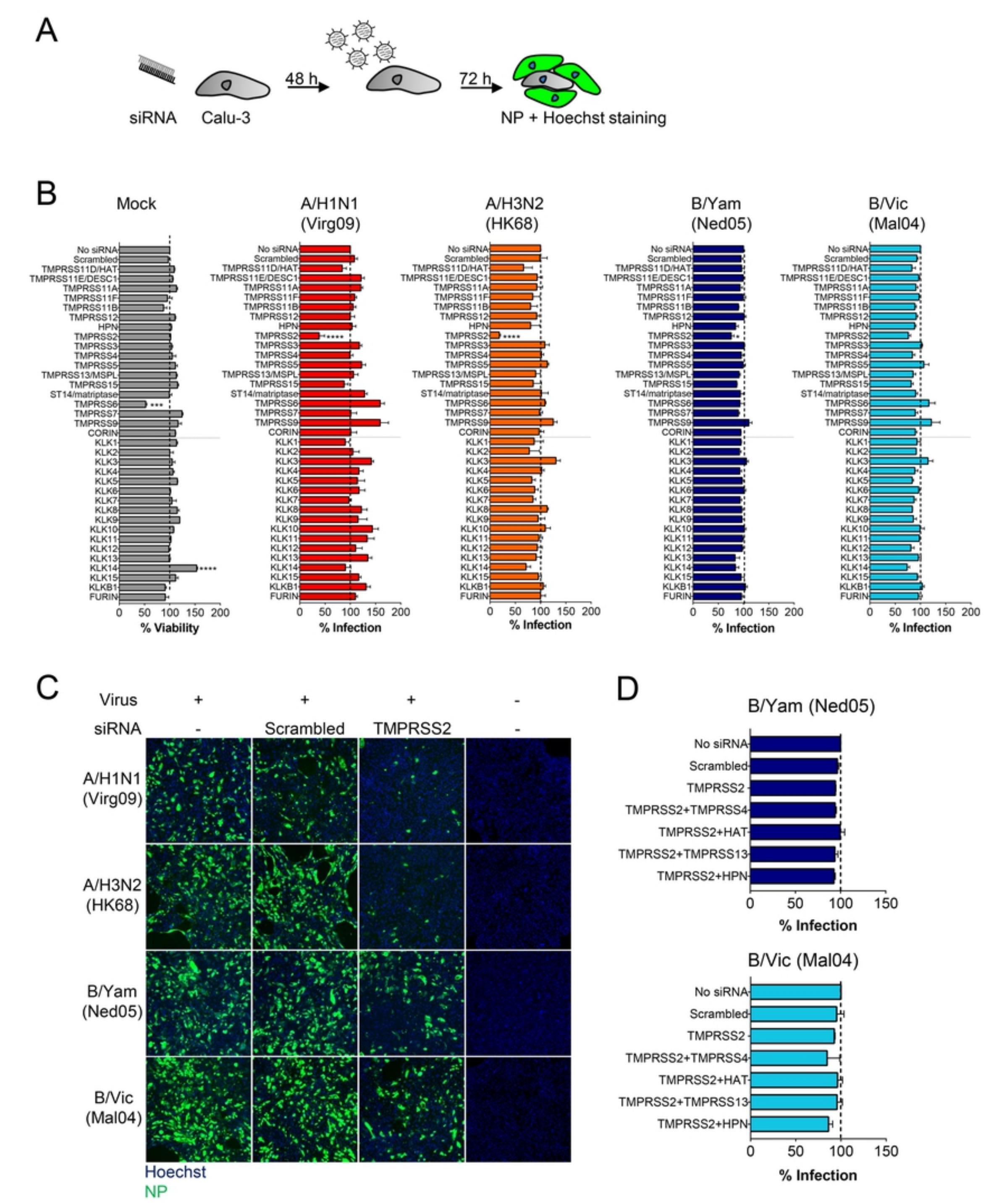
A
siRNA
Calu-3
48 h
72 h
NP + Hoechst staining
B
Mock
A/H1N1 (Virg09)
A/H3N2 (HK68)
B/Yam (Ned05)
B/Vic (Mal04)
No siRNA
Scrambled
TMPRSS11D/HAT
TMPRSS11E/DESC1
TMPRSS11A
TMPRSS11F
TMPRSS11B
TMPRSS12
HPN
TMPRSS2
TMPRSS3
TMPRSS4
TMPRSS5
TMPRSS13/MSPL
TMPRSS15
ST14/matriptase
TMPRSS6
TMPRSS7
TMPRSS9
CORIN
KLK1
KLK2
KLK3
KLK4
KLK5
KLK6
KLK7
KLK8
KLK9
KLK10
KLK11
KLK12
KLK13
KLK14
KLK15
KLKB1
FURIN
0 50 100 150 200
% Viability
% Infection
C
Virus + + + -
siRNA - Scrambled TMPRSS2 -
A/H1N1 (Virg09)
A/H3N2 (HK68)
B/Yam (Ned05)
B/Vic (Mal04)
Hoechst
NP
D
B/Yam (Ned05)
No siRNA
Scrambled
TMPRSS2
TMPRSS2+TMPRSS4
TMPRSS2+HAT
TMPRSS2+TMPRSS13
TMPRSS2+HPN
0 50 100 150
% Infection
B/Vic (Mal04)
No siRNA
Scrambled
TMPRSS2
TMPRSS2+TMPRSS4
TMPRSS2+HAT
TMPRSS2+TMPRSS13
TMPRSS2+HPN
0 50 100 150
% Infection

Fig 5

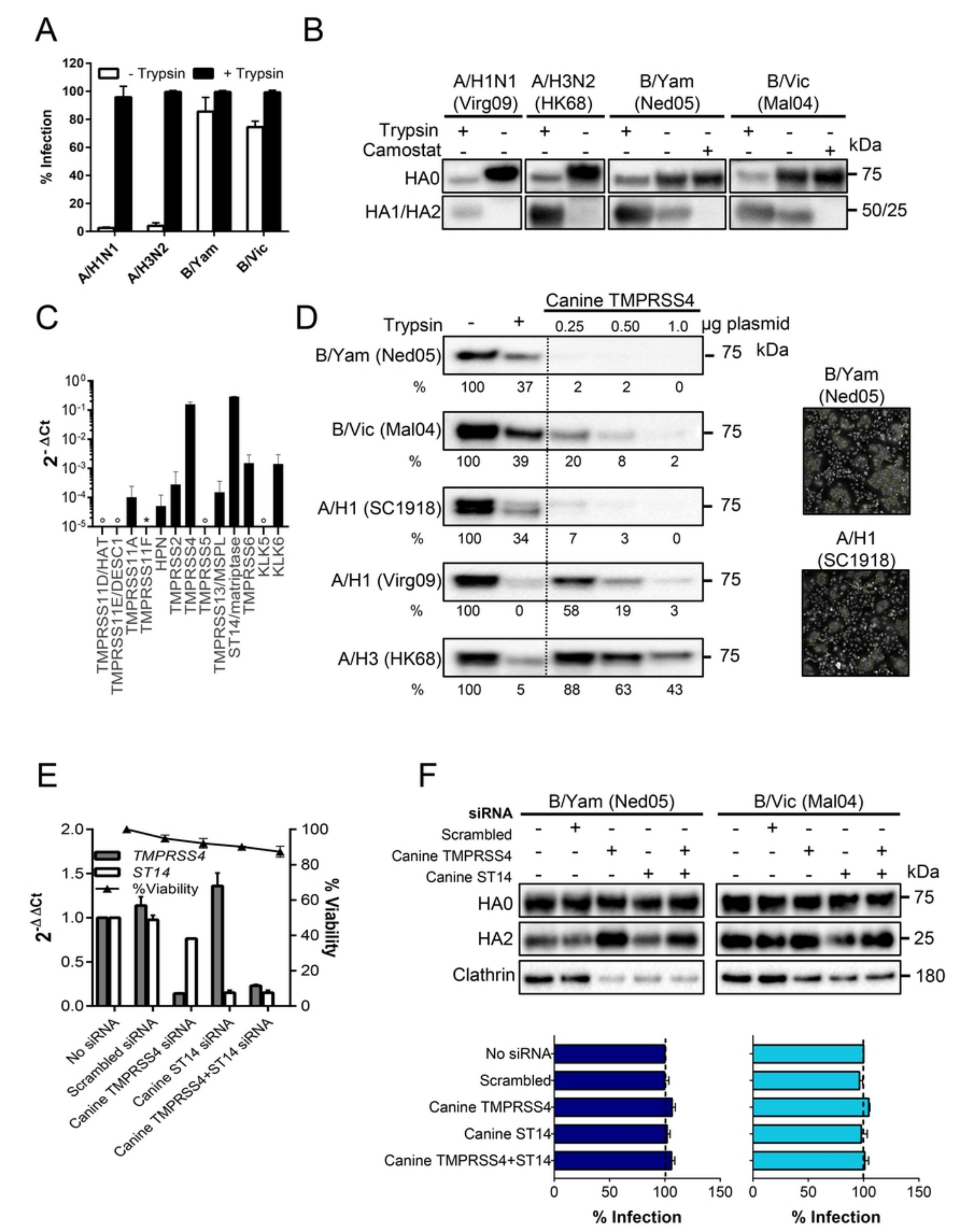
A
- Trypsin
+ Trypsin
% Infection
A/H1N1
A/H3N2
B/Yam
B/Vic
B
A/H1N1 (Virg09)
A/H3N2 (HK68)
B/Yam (Ned05)
B/Vic (Mal04)
Trypsin
Camostat
kDa
HA0
HA1/HA2
75
50/25
C
2-ΔCt
TMPRSS11D/HAT
TMPRSS11E/DESC1
TMPRSS11A
TMPRSS11F
HPN
TMPRSS2
TMPRSS4
TMPRSS5
TMPRSS13/MSPL
ST14/matriptase
TMPRSS6
KLK5
KLK6
D
Canine TMPRSS4
Trypsin
0.25
0.50
1.0
µg plasmid
B/Yam (Ned05)
B/Vic (Mal04)
A/H1 (SC1918)
A/H1 (Virg09)
A/H3 (HK68)
%
B/Yam (Ned05)
A/H1 (SC1918)
E
2-ΔΔCt
% Viability
TMPRSS4
ST14
%Viability
No siRNA
Scrambled siRNA
Canine TMPRSS4 siRNA
Canine ST14 siRNA
Canine TMPRSS4+ST14 siRNA
F
siRNA
B/Yam (Ned05)
B/Vic (Mal04)
Scrambled
Canine TMPRSS4
Canine ST14
kDa
HA0
HA2
Clathrin
75
25
180
No siRNA
Scrambled
Canine TMPRSS4
Canine ST14
Canine TMPRSS4+ST14
% Infection
% Infection

Fig 6

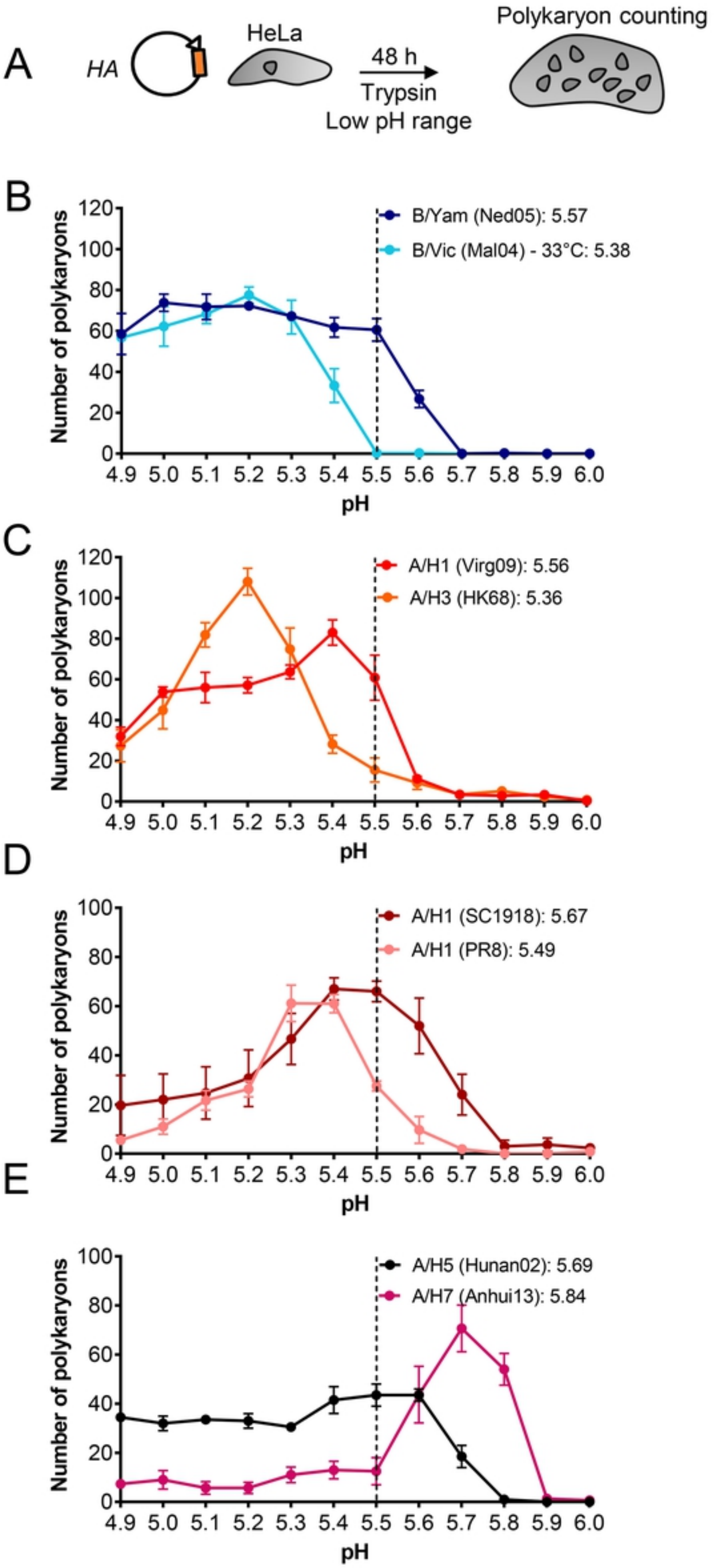
A
HA
HeLa
48 h
Trypsin
Low pH range
Polykaryon counting
B
B/Yam (Ned05): 5.57
B/Vic (Mal04) - 33°C: 5.38
Number of polykaryons
pH
C
A/H1 (Virg09): 5.56
A/H3 (HK68): 5.36
Number of polykaryons
pH
D
A/H1 (SC1918): 5.67
A/H1 (PR8): 5.49
Number of polykaryons
pH
E
A/H5 (Hunan02): 5.69
A/H7 (Anhui13): 5.84
Number of polykaryons
pH

Fig 7

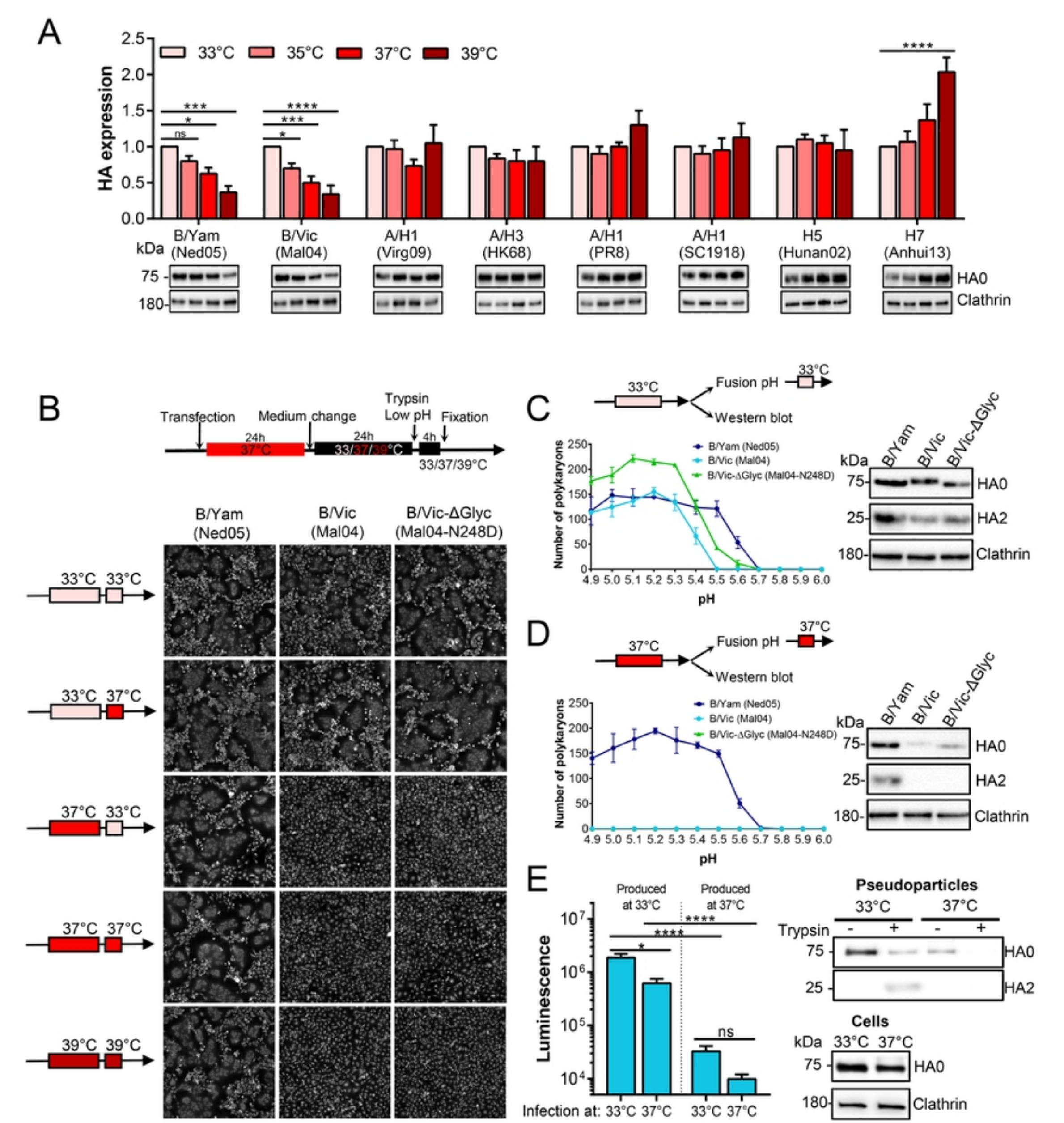
A
33°C
35°C
37°C
39°C
HA expression
B/Yam (Ned05)
B/Vic (Mal04)
A/H1 (Virg09)
A/H3 (HK68)
A/H1 (PR8)
A/H1 (SC1918)
H5 (Hunan02)
H7 (Anhui13)
kDa
HA0
Clathrin
B
Transfection
Medium change
Trypsin Low pH
Fixation
24h 37°C
24h 33/37/39°C
4h
33/37/39°C
B/Yam (Ned05)
B/Vic (Mal04)
B/Vic-ΔGlyc (Mal04-N248D)
33°C 33°C
33°C 37°C
37°C 33°C
37°C 37°C
39°C 39°C
C
33°C
Fusion pH
Western blot
Number of polykaryons
pH
B/Yam (Ned05)
B/Vic (Mal04)
B/Vic-ΔGlyc (Mal04-N248D)
HA0
HA2
Clathrin
D
37°C
Fusion pH
Western blot
E
Produced at 33°C
Produced at 37°C
Luminescence
Infection at: 33°C 37°C 33°C 37°C
Pseudoparticles
Trypsin
Cells

Fig 8